North Atlantic Oscillation (NAO) in the Paleoclimate Modelling Intercomparison Project (PMIP)

Anni Zhao[1], Chris Brierley[2], Venni Arra[2], Xiaoxu Shi[3], and Yongyun Hu[1]

[1]Department of Atmospheric and Oceanic Sciences, School of Physics, Peking University, Beijing, 100871, China
[2]Department of Geography, University College London, London, WC1E 6BT, UK
[3]Southern Marine Science and Engineering Guangdong Laboratory, Zhuhai, 519082, China

Correspondence: Yongyun Hu (yyhu@pku.edu.cn)

Abstract. The North Atlantic Oscillation (NAO) is one of the main modes of climate variability and the dominant mode of large-scale atmospheric variability in the North Atlantic basin and has large impacts on the European climate, whose future behaviour remains uncertain. Here we assess the NAO response in past and future climates by looking at a comprehensive set of coupled model simulations performed by the Paleoclimate Model Intercomparison Project (PMIP) and the Coupled Model

5   Intercomparison Project (CMIP) for four experiments: the mid-Holocene (6 ka; *midHolocene*), the Last Glacial Maximum (21 ka; *lgm*), the last interglacial (127 ka; *lig127k*) and an idealised future warming scenario with abrupt quadrupled CO_2. Although there are various setups across experiments, the *midHolocene* and *lig127k* are mainly characterised by altered orbital configurations, inducing variations in the seasonal cycle, and the *lgm* and *abrupt4xCO2* are mainly characterised by various GHG forcing that induces great global temperature change. Our results show that the NAO is sensitive to GHG-forcing-induced

10   temperature changes but not the orbital configurations. NAO weakens in response to cooling and strengthens to warming. The associated teleconnections change consistently with the theory and are sensitive to the change in NAO amplitude. The two orbital experiments do not show a clear change in associated temperature and precipitation. The weakened NAO in the *lgm* is associated with a cooler and drier northern Europe, while the enhanced NAO in the *abrupt4xCO2* causes a warmer and wetter northern Europe as compared to the *piControl*. No clear relationship is found in the ENSO-NAO teleconnection.

15   **1 Introduction**

The North Atlantic Oscillation (NAO), characterised by seesaw sea level pressure anomalies between the Icelandic Low and the Azores High, represents one of the main modes of climate variability and the dominant mode of large-scale atmospheric variability in the North Atlantic basin (Hurrell et al., 2003). It affects climate throughout all seasons, most pronounced during boreal winter (Walker and Bliss, 1932). There is ongoing debate on the relationship between the NAO and the North Annular

20   Mode (NAM, also known as the Arctic Oscillation): some studies interpret the NAM as a statistical artefact of two independent regional modes (NAO and the Pacific-North American pattern), and thus viewing the NAO as a stand-alone mode (Ambaum et al., 2001); while others view the NAO as a regional expression of the NAM (e.g. Thompson and Wallace, 1998; Kimoto et al., 2001) and do not distinguish between the two. The latest phase of the Intergovernmental Panel on Climate Change (IPCC AR6)

often considers the NAM and the NAO as the same entity, as the NAO can explain most of the variance in zonally-averaged
25 hemispheric circulation and exhibits a high correlation in associated time-series (IPCC, 2021b).

NAO is predominantly driven by the internal atmospheric variability of mid-latitude dynamics (Lorenz and Hartmann, 2003)
related to the interaction between eddy-mean flow (Feldstein and Franzke, 2017; Kimoto et al., 2001) and the coupling between
troposphere and stratosphere (Wang and Ting, 2022; Omrani et al., 2022), and the coupling among atmosphere, land, and ocean
(Marshall et al., 2001). Various mechanisms play important roles in shorter to longer-term NAO variability (Stephenson et al.,
30 2006), including sea surface temperature (SST) (Mosedale et al., 2006; Hurrell et al., 2004), greenhouse gas (GHG) forcing
(Stephenson et al., 2006; Barnes and Polvani, 2013), sea ice (Pedersen et al., 2016; Smith et al., 2017), and snow cover changes
(Henderson et al., 2018; Spencer and Essery, 2016). The NAO strongly impacts regional surface climate variables (Woollings
et al., 2015), notably modulating surface air temperature over Europe (Hurrell, 1995). The interplay between the two pressure
systems creates a pressure gradient that influences the strength and direction of westerly winds and storm tracks across the
35 North Atlantic. The phases of NAO significantly influence the temperature and precipitation variability over the North Atlantic
and Eurasia, as well as related westerly winds and storm tracks (Woollings et al., 2014). In its positive phase, the NAO is
formed by relatively stronger low pressure over Iceland in the mid to high latitudes and stronger high pressure over the Azores
in the subtropics, leading to an enhanced and northward shift of the jet stream, strengthened trade winds, and a northward shift
of extra-tropical storms. The positive NAO typically results in a warmer and wetter northern Europe and a colder and drier
40 Mediterranean. Conversely, the negative phase of the NAO shows the reverse change in pressure systems, leading to a wavier
jet stream that extends southward and a southward shift of storms, resulting in a colder northern Europe and a warmer southern
Europe.

Research around changes in the NAO involves some awkward terminology. Here we consider the NAO to be a mode of
variability, which can be described by the interannual changes in the NAO index. Changes in the mean state of the Icelandic
45 Low and Azores High will also project onto the pattern of that mode of variability - leading to secular shifts in the NAO
index (i.e. shift in the mean state of the NAO), even if the oscillation itself remains the same. These are easy to distinguish
in equilibrated climate model experiments, such as those used here. However, it is harder when looking at continuous NAO
indices that capture a large range of frequencies, such as from palaeoclimate reconstructions or long transient simulations.

Several studies have carried out proxy-based reconstructed NAO (e.g. Vinther et al., 2003; Cook et al., 2019), though the
50 reconstructions are limited by significant uncertainties arising from the limitations of archives and chronologies (Hernández
et al., 2020), diverse methodologies (Michel et al., 2020), or the time scale effect on NAO variability (Woollings et al., 2015).
For example, a positive NAO-like configuration was suggested during the mid-Holocene (6 ka) based on reconstructed ter-
restrial temperature over Europe (Mauri et al., 2014) and SSTs (Rimbu et al., 2003). Earlier studies have explored the NAO
in paleoclimate simulations; however, the exact behaviour of NAO remains uncertain. The mid-Holocene simulations of the
55 Palaeoclimate Modeling Intercomparison Project 2 (PMIP2) show various changes in NAO variability as compared to the pre-
industrial condition, as reduced (Lü et al., 2010), no change (Otto-Bliesner et al., 2006), or enhanced (Gladstone et al., 2005),
the results of the PMIP3 are also model-dependent (Găinuşă-Bogdan et al., 2020). Under the cooler-than-present condition
of the Last Glacial Maximum (LGM; 21 ka), simulations show that the NAO pattern and variability weaken drastically in

simulations, and the centres of the NAO pattern shift southward compared to both the pre-industrial and the mid-Holocene (Lü
60 et al., 2010; Otto-Bliesner et al., 2006).

Future simulations predict a more positive mean state of the NAO index, although the response is highly model dependent
(Miller et al., 2006; Osborn, 2004; Bader et al., 2011). The mean state of the NAO index is projected to shift positively under
high-emission scenarios while showing less robust change under low-emission scenarios by the end of the 21st century, with
a large diversity across the Coupled Model Intercomparison Project (CMIP) simulations (Lee et al., 2021). The large spread
65 is partly due to the contrasting influences of the negative phase of the NAO induced by Arctic amplification (Harvey et al.,
2015; Peings et al., 2017; Screen et al., 2018) and the positive phase associated with enhanced warming in the tropical upper-
troposphere (Vallis et al., 2015) in particular models in response to anthropogenic forcing (Harvey et al., 2014, 2015; Vallis
et al., 2015; Oudar et al., 2017).

In this study, we look at simulated NAO change by the new generation of climate models for three PMIP experiments and
70 a CMIP CO_2 scenario experiment to assess NAO change through time. The PMIP experiments represent a colder LGM and
two past climates with altered orbital configurations, the last interglacial (LIG; 127 ka) and the mid-Holocene. The CMIP CO_2
scenario experiment is an idealised warming projection designed with abrupt quadrupled CO_2. Sect. 2 introduces the models,
experimental design, and analysis methods. A comparison between the *piControl* experiment with observation is provided
in Sect. 3 for model evaluation. Sect. 4 describes changes in the mean state relative to the *piControl*. Sect. 5 presents the
75 description of the change in NAO and the associated discussion. NAO teleconnections change, and discussion is given in Sect.
6. A brief conclusion is provided at the end as Sect. 7. Comparison between PMIP simulations with proxy data is not the aim of
this study, and it has been done in assessing single experiments (see Brierley et al., 2020; Otto-Bliesner et al., 2021; Kageyama
et al., 2021), so it will not be discussed in detail below.

2   Methods

80 This study involves a bunch of simulations across 2 CMIP/PMIP generations, 5 experiments and 34 climate models (Table 1).
Studies on individual experiments (Brierley et al., 2020; Otto-Bliesner et al., 2021; Kageyama et al., 2021) and single-model
evaluations have been done by model groups (e.g. Otto-Bliesner et al., 2020). Therefore, we will keep the description of models
and experimental design brief here, whilst references will be provided to find details.

2.1   Models

85 State-of-the-art coupled global climate models represent the climate system through physical equations based on the physical,
chemical and biological properties of the system's components, their interactions and feedback, and other known properties.
Climate models are tools to investigate how the climate responds to various climate forcings and project future climate change
in different scenarios. The CMIP has become a significant international multi-model research activity to investigate the Earth
system response to forcing, evaluating the state-of-the-art coupled global climate models and assessing future climate changes
90 and their uncertainties in scenarios (Eyring et al., 2016; Taylor et al., 2012). Simulations from the PMIP look at the past and

serve as out-of-sample tests to study the roles of forcings and their feedbacks that establish the palaeoclimate and to evaluate the performance of models that are used to project future climate changes (Kageyama et al., 2018). Here, we choose the models that have completed the *piControl* simulations and at least one of the PMIP simulations (see Sect. 2.2) and have provided monthly surface temperature, precipitation and sea level pressure (SLP) for at least 30 years for all the simulations. Table 1 lists the 34 chosen models and their participation in the six experiments (see Sect. 2.2). Further details of the model design can be found in the listed references in Table 1 here and Table 9.A.1 of Flato et al. (2013) for the CMIP5 models and Table AII.5 of IPCC (2021a) for the CMIP6 models.

2.2 Experimental design

This study uses simulations from six experiments with the protocols defined under the CMIP (Taylor et al., 2012; Eyring et al., 2016) or the PMIP (Kageyama et al., 2018): a pre-industrial control, one idealised CO_2-forced future warming scenario and three past climate experiments which include a colder *lgm* and two altered orbital configurations *midHolocene* and *lig127k*. Model participation in each experiment is detailed in Table 1.

The DECK *piControl* was performed by all selected models, employing coupled atmosphere-ocean and boundary conditions approximately constant to 1850CE (Eyring et al., 2016). Depending on the individual model design, aerosol, vegetation, and ice sheet configurations are either interactive or prescribed as modern conditions. The CMIP6 *piControl* uses more realistic GHG concentrations and a lower solar constant compared to its earlier generation, the CMIP5. The *piControl* serves as a baseline for assessing changes in other experiments. Model groups run their *piControl* simulations for a few hundred to a few thousand model years to reach an equilibrium state.

The idealised CO_2-forced experiment, *abrupt4xCO2*, is also a requirement of the DECK CMIP experiments (Eyring et al., 2016). It is designed to reveal the basic feedback response of a model to high GHG forcing (Eyring et al., 2016), by having the atmospheric CO_2 concentration suddenly and immediately quadruple relative to the 1850 CE condition prescribed in the *piControl* at the beginning and then maintaining constant (Eyring et al., 2016). The *abrupt4xCO2* simulations enable the estimation of a model's equilibrium climate sensitivity (Zelinka et al., 2020). Its protocol remains unchanged as in the CMIP5, facilitating comparisons across CMIP generations.

The *lgm* experiment is designed to examine the effect of altered ice sheets, continental extent due to reduction in sea level, and lower GHG forcings (Kageyama et al., 2018). The major difference between the PMIP3 and PMIP4 *lgm* simulations is the choice of the prescribed ice sheets. While the PMIP3 simulations all used the same composite ice-sheet reconstructions(Abe-Ouchi et al., 2015), the PMIP4 simulations chose one of the three as summarised in Kageyama et al. (2021): the original PMIP3-CMIP5 ice sheet (Abe-Ouchi et al., 2015), GLAC-1D (Ivanovic et al., 2016) and ICE-6G_C (Peltier et al., 2015; Argus et al., 2014). Although these reconstructions have similar ice sheet extent, they differ in the heights of the Laurentide, Fennoscandian, and West Antarctica ice sheets.

The *midHolocene* and *lig127k* experiments are designed to examine the climate system responses to orbital forcings that differ from the pre-industrial (Kageyama et al., 2018). The experimental designs for the two experiments are outlined by Otto-Bliesner et al. (2017). The *midHolocene*, included since the beginning of the PMIP (Joussaume and Taylor, 1995; Braconnot

125   et al., 2000), set to an orbital configuration at 6 ka following Berger (1978) and Berger and Loutre (1991). The orbit at 6 ka was characterised by larger obliquity, and its perihelion occurred near the boreal autumn equinox. The prescribed GHG concentrations in the PMIP4 *midHolocene* use more realistic concentrations derived from ice cores and observations (Otto-Bliesner et al., 2017) than the PMIP3, which contributes to a decrease of 0.3 W m^{-2} in effective radiative forcing (Otto-Bliesner et al., 2017). The *lig127k* uses the orbital configuration at 127 ka (Berger and Loutre, 1991), characterised by a larger

130   eccentricity than the pre-industrial and its perihelion close to the boreal summer solstice. Both periods were characterised by receiving more insolation at the top of the atmosphere (TOA) in the Northern Hemisphere during JJA and less incoming solar radiation in both hemispheres during DJF compared to 1850 CE, with the LIG having stronger orbital forcing than the mid-Holocene.

2.3   Analysis and definitions

135   The analysis in this work follows the workflow described by Zhao et al. (2022). We create a curated replica of the relevant simulation outputs available on the System Grid Federation (ESGF; Balaji et al., 2018), which stores the CMIP6 outputs in a standardised format (Juckes et al., 2020). Digital Object Identifier (doi) for each simulation downloaded from the ESGF can be found in the Supplement. We also require some simulations from the model groups if they are not available on the ESGF. Then we apply calendar adjustment on the *midHolocene*, *lig127k* and *lgm* monthly output that re-aggregate the monthly output from

140   a present-day calendar to those representing the past via the PaleoCalAdjust software by Bartlein and Shafer (2019). In order to compare with equilibrium simulations, we take the last 50 model years of the *abrupt4xCO2* simulations in analysis. The Climate Variability Diagnostics Package (CVDP; Brierley and Wainer, 2018) had been modified for palaeoclimate purposes (Brierley and Wainer, 2018). We run the modified CVDP on each simulation to calculate multiple pertinent time series and spatial fields. The CVDP outputs have been regridded to 1° by 1° before analysing to eliminate the effects of different initial

145   resolutions across all the models. Multi-model mean anomalies take the average of regridded anomaly (*experiment - piControl*) across the ensemble members (Brierley and Wainer, 2018). Please see Zhao et al. (2022) for more details. We evaluate ensemble consistency as at least two-thirds of the models agree on the sign of the multi-model mean. Results of the PMIP4 and PMIP3 have not shown fundamental differences in statistics (Brierley et al., 2020; Kageyama et al., 2021), so we, therefore, combine the two indistinguishable phases in the purpose of enlarging the size of ensembles, which have been adopted in analysing

150   ENSO (Brown et al., 2020) and Indian dipole (Brierley et al., 2023) across experiments.

    NAO can be defined based on the principal component (PC-based) as the leading empirical orthogonal function (EOF) of SLP variance during boreal winter over the North Atlantic-Europe sector (IPCC, 2021b), or based on observations from fixed locations as the difference of normalised SLP anomalies between stations located in the Azores-Ponta Delgada and Iceland (Jones et al., 1997) or the difference between London and Paris (Cornes et al., 2013). Here, we adopt the definition of NAO as

155   the leading empirical orthogonal function (EOF) of DJF SLP anomalies over the Northern Hemisphere north of 20°N to 80°N and 90°W to 40°E (hereafter referred to as the NAO pattern). The NAO index is the normalised PC time series of the EOF. Instead of using the NAO index, we use the amplitude of NAO to show its strength, which is measured as the standard deviation of the renormalised PC time series (i.e. the NAO index times the standard deviation of the spatial NAO pattern over the region).

We also present spatial patterns associated with the NAO by linearly regressing the monthly temperature and precipitation onto

160 the NAO index to evaluate the association between the NAO and surface climate variables (Brierley and Wainer, 2018). We also examine the similarity between the NAO and the NAM in the PMIP experiments. All the experiments show that NAM and NAO are strongly correlated in the time series of the NAO indices, explained by variance and amplitude (not shown). Therefore, the following sections do not distinguish the NAO from the NAM.

3   Comparison with observations

165 Before looking at the response in experiments, we first evaluate the ability of the CMIP models used in this study to reproduce climate states during the pre-industrial period by comparing the *piControl* simulations with the C20 Reanalysis dataset (Compo et al., 2011), as shown in Figure 1. Models generally capture the spatial pattern of observed mean DJF temperature, but bias in producing too cold Arctic, especially over Greenland and Nunavut (Figure 1a, b). The cold bias has been detected by earlier PMIP analyses on a single experiment (Brierley et al., 2020; Otto-Bliesner et al., 2021), both showing a large spread

170 across the models in Arctic regions between 60°N and 90°N. The bias is partly associated with the model's representation of cloud radiative processes (Zhang et al., 2023) and atmospheric dynamics (Hall et al., 2021) and may also be affected by Arctic hydrography (Khosravi et al., 2022). Figure 1c and d show that models capture the DJF mean precipitation pattern over the North Atlantic Ocean, though they underestimate the amount of precipitation and shift the maximum location westward slightly as compared to the observation. The simulated SLP generally agrees with the observation (Figure 1 e and f), although

175 it produces lower pressure along the coast of Greenland.

The NAO is the leading EOF of DJF SLP over the North Atlantic-Europe sector (see Sect. 2.3), whose simulated pattern shows a positive phase during the pre-industrial (Figure 1g, h), consistent with observations but with significant negative anomalies extended further into the centre of Greenland and an underestimation of positive anomalies around 30-40°N North Atlantic Ocean. In the *piControl* simulations, the NAO explains 41.5% (34.3%-52.0%) of the total variance, slightly less than

180 42.3% from observation. The *piControl* surface air temperature imprint of the NAO shows a pattern of warmer mid-latitudes and colder subpolar and subtropical regions than the observation (Figure 1i and j), with the effect of a stronger jet stream located further north, stronger trade winds and northward shift of extratropical storms associated with a positive phase of NAO IPCC (2021b). The related northward shift of storm tracks with positive NAO phases results in a wetter northern Europe, a drier southern Europe and a northward shift of precipitation over the ocean. Both observations and models capture the pattern

185 (Figure 1k, l), but the simulated pattern is smoother than the observation with underestimated change magnitudes.

4   Change in mean state

First the changes in mean climate over the North Atlantic are evaluated for each experiment, relative to the *piControl* simulations. Figure 2 summarises the DJF response of the experiments to the two forcings for SAT (left column), precipitation (middle column), and SLP (right column). We present and discuss the response of *midHolocene* and *lig127k* experiments to-

190 gether firstly to show the climate response to orbital forcing, and then present those of the *lgm* and *abrupt4xCO2* experiments for response to GHG forcing, though the *lgm* experiment also involves the response to the ice sheet.

The orbit configuration was characterised by larger obliquity at 6 ka and larger eccentricity at 127 ka than pre-industrial ones. The perihelion at 6 ka occurred near the boreal autumn equinox. At 127 ka, it occurred close to the boreal summer solstice rather than near the boreal winter solstice during the pre-industrial (Berger and Loutre, 1991). Both periods were

195 characterised by receiving less incoming solar radiation globally during DJF compared to 1850 CE, with a stronger reduction at 127 ka, suggesting an expectation of cooling in both experiments. The meridional SAT gradients of the *midHolocene* and *lig127k* experiments are weaker than the *piControl*, and the *lig127k* displays a stronger signal (Figure 2a, d). The DJF mean temperature change averaged over the N. Atlantic sector in the *midHolocene* experiment is 0.07°C cooler than the *piControl*. The cooling is stronger in the *lig127k* experiment at -0.52°C. Both experiments produce polar amplification, though the signal

200 is inconsistent across the ensembles. The *lig127k* simulations show a large spread across the models in producing Arctic warming, and the *midHolocene* simulations show a larger ensemble spread over the whole region of the North Atlantic sector. The Arctic warming during the boreal winter suggests other important processes, e.g. polar amplification with smaller and thinner sea ice in the Arctic (Serreze and Barry, 2011) and ocean memory (Marino et al., 2015; Govin et al., 2012).

Meanwhile, both experiments do not incorporate some regional processes that can cause regional coolings, e.g. the *lig127k*

205 simulations did not include meltwater from ice sheets over Scandinavia and Canada related to the cooling in the Nordic Seas and south of Greenland shown by LIG reconstruction (Barlow et al., 2018; Otto-Bliesner et al., 2021). Earlier studies have compared the experiments with reconstruction and have confirmed that both experiments underestimate the Arctic warming (Brierley et al., 2020; Otto-Bliesner et al., 2021). The underestimated mid-Holocene Arctic warming has existed since the PMIP3-CMIP5 (Harrison et al., 2015; Yoshimori and Suzuki, 2019). The regional temperature bias in the CMIP5 *midHolocene*,

210 *piControl* and *historical* are similar (Ackerley et al., 2017; Harrison et al., 2015), which indicates the persistent errors in representing the climate system. The Euro-Atlantic precipitation fields show a drier Europe and an apparent drying off of the North American east coast in both experiments as compared to the *piControl* (Figure 2b, e). There is a wetting over the rest of the Atlantic in the ensemble average, although the models do not all agree on the sign of the change. The signal of multi-model mean precipitation change is affected by NorESM2-LM, which produces a much larger precipitation increase north of 40°N

215 than other models in both experiments. Figure 2c, f shows that SLP increases over lower latitudes and decreases over high latitudes.

The LGM was characterised by a colder climate with a global mean cooling of 5–7°C (Gulev et al., 2021) and large ice sheets covering the mid- to high-latitudes in the Northern Hemisphere (Clark and Mix, 2002; Clark et al., 2009). The averaged DJF cooling over the North Atlantic sector is -9.86°C in the *lgm* simulations compared to the *piControl*. The *lgm* simulations

220 show consistent cooling over the sector with a greater temperature decrease over land than over sea (Figure 2g). The greatest cooling is found over the Norwegian and Barents Seas and parts of Scandinavia and North America, which reflects the change in surface height and albedo related to ice sheet change (Kageyama et al., 2021). The cooling is also partly affected by the advection of the cold temperature anomalies downwind of the ice sheets (Kageyama et al., 2021) and is partly related to a weakened Atlantic meridional overturning circulation (AMOC) (Jonkers et al., 2023). Though the cooling signal is consistent,

225　the ensemble shows a large spread in simulating the magnitude of cooling affected by the choice of ice sheets of the PMIP3 simulations shown in Kageyama et al. (2021). Shi et al. (2023) decomposed the contribution of individual boundary conditions and forcings to the LGM cooling and found that the cooling over the sea within the region is mainly due to the GHG forcings and that over the continent is due to changes in ice sheets. The *abrupt4xCO2* simulations show a contrasting signal to the LGM by showing consistent warming over the whole North Atlantic region with greater warming over land (Figure 2j). The

230　*abrupt4xCO2* experiment shows a warming of 6.41°C over the sector. The weakest warming appears over the ocean south of Iceland, where the AMOC condenses. Earlier studies suggest the AMOC weakening in the *abrupt4xCO2* experiment in response to warming (Zhu et al., 2023; Madan et al., 2024). The *lgm* simulations show enhanced precipitation over mid-latitudes North Atlantic Ocean as compared to the *piControl*, but the signal is not consistent across the ensemble (Figure 2h). The switch of precipitation change signal represents a northward shift of the jet stream (Figure 2i) relative to the *piControl*,

235　whereas the inconsistency shows the uncertainty in producing the location of the jet stream. Though the increase in the multi-model mean of *abrupt4xCO2* precipitation change is consistent, the spatial pattern of the change by individual models is complex. The weakened precipitation south of Iceland is inconsistent across the *abrupt4xCO2* ensemble (Figure 2i), as about half of the models produce such a reduction. The SLP increases uniformly in the *lgm* simulations, consistent with the enhanced SAT cooling (Figure 2g). The higher SLP over the polar regions, coupled with a cooler and dryer climate, is related to the large

240　Laurentide ice sheet (Otto-Bliesner et al., 2006). The pattern of *abrupt4xCO2* SLP change (Figure 2l) is not consistent with temperature change. The inactive prescribed Greenland ice sheets in simulations (Eyring et al., 2016) cause the SLP increase over the region.

5 Change in NAO

In the *piControl* simulations, the NAO explains 41.5% of DJF SLP variance and shows a distinguishable positive phase with

245　a strong negative SLP centre over the northeast of Iceland and a positive centre over the northeast of the Azores (Sect. 3). Notably, 9 out of the 34 models display an eastward shifted positive centre over Europe along with varying degrees of pattern strength, and UofT-CCSM-4 produces dipole positive centres over the Mediterranean and the central USA. The DJF NAO time series has an average amplitude of 2.27 hPa in the *piControl* simulations, ranging from 0.93 hPa (CSIRO-Mk3-6-0) to 2.99 hPa (CCSM4).

250　The NAO patterns of the two orbital experiments are not distinguishable from the *piControl* (Figure 3a, c). The similarity in the NAO pattern between the *midHolocene* and the *piControl* agrees with the findings of earlier modelling studies (Otto-Bliesner et al., 2006; Gladstone et al., 2005; Stephenson et al., 2006). It is also consistent with the PMIP2 simulations (Lü et al., 2010) that found the mid-Holocene leading EOF of DJF SLP is similar to the PI. Models produce complex changes in the NAO pattern in both experiments and show a spread south of Greenland and Iceland near 50°N (Figure 3b, d). Of the

255　32 models, 11 display a clear weakening and 7 show an enhanced positive NAO phase in the *midHolocene*, respectively, as compared to the *piControl*; a similar result of spatial change occurs for the *lig127k* experiment, as 6 (5) out of the 14 models display weakness (enhancement) in the *lig127k* as compared to the *piControl* (not shown). The average percentage of explained

variance during the *midHolocene* is 42.4% (33.2-51.8%), whose range is close to the *piControl* (Figure 4). No clear changes in explained variance stay consistent with Gladstone et al. (2005), which, in conjunction with inter-model inconsistencies, leads

260 to uncertainties about the mid-Holocene NAO behaviour. Changes in explained variance vary across the ensemble (Figure 4b), ranging from -7.1% by EC-Earth-2-2 to 10.1% by UofT-CCSM-4. In the *lig127k* simulations, models display an averaged explained variance at 43.4% (38.3% to 47.7%), different from the 42.7% (35.7-52.0%) in the corresponding *piControl* simulations. Changes in explained variance by individual models vary across the ensemble and do not show a trend (Figure 4b). The NAO amplitude in the *midHolocene* simulations is 2.31 hPa (0.77-3.15 hPa). The range and distribution of the *midHolocene*

265 NAO amplitude are similar to those of the *piControl* (Figure 5), though the differences between *midHolocene* and *piControl* by individual models range from -0.30 hPa (EC-Earth3-LR) to 0.79 hPa (CSIRO-MK3-6-0). Though 19 out of 32 models present increased NAO amplitude, the ensemble mean change in the NAO amplitude is 0.06 hPa. The slight increase is largely affected by CSIRO-MK3-6-0, UofT-CCSM4 and HadGEM2-CC, which contribute an intensification at 0.79 hPa, 0.50 hPa and 0.43 hPa, respectively. The *lig127k* NAO amplitude is 2.18 hPa, similar to the *piControl* at 2.28 hPa with a more concentrated

270 distribution (Figure 5). The results of the two orbital-driven experiments suggest that the NAO response is unaffected by the seasonal variation induced by altered orbital configurations.

In the *lgm* experiment, the NAO weakens than the *piControl* (Figure 3e). There is a southward shift of both the negative and positive centres of the NAO as compared to the *piControl* (Figure 3e), though with a large model spread over the N. Atlantic Ocean between 40°N and 65°N (Figure 3f). The weakened NAO and centre shifts in the *lgm* are consistent with the

275 results of Lü et al. (2010) and Otto-Bliesner et al. (2006). Models show large variations in producing the location of positive and negative centres of the NAO. 8 out of the 13 models display the switch of signal between 50°N and 60°N, where IPSL-CM5A-LR displays its negative centre while COSMOS-ASO shows its positive centre. The NAO explains 39.6% (33-48.5%) of SLP variability in the *lgm* (Figure4a) that is -1.6% less than the corresponding *piControl* simulations. The majority of the models show a reduction in explained variance (Figure 4b), except FGOALS-g2 (9.2%), MIROC-ES2L (8.7%) and INM-

280 CM4-8 (3.3%). The *lgm* NAO amplitude is 1.58 (1.02-2.55) hPa, which is 0.59 hPa weaker than the *piControl* (Figure 5). UofT-CCSM-4 contributes to the largest weakness in amplitude at -1.61 hPa. Only INM-CM4-8, MIROC-ES2L and MIROC-ESM contribute to enhanced amplitude in the *lgm* simulations. Quartiles and median in Figure 5 show a general reduction in *lgm* amplitude than the *piControl*, which implies a weaker NAO in the *lgm*. The weakness is partly related to the presence of the Laurentide and Scandinavian ice sheets (Braconnot et al., 2007). The *abrupt4xCO2* experiment shows the opposite change

285 in the NAO by showing enhancement and a slight northward shift in centres than the *piControl* (Figs 3g,h). Models produce increased explained variance (Figure 4) and stronger amplitude (Figure5) than the *piControl*. The *abrupt4xCO2* simulations explain 43.2% (32.9-52.6%) of the SLP anomalies, which are 2.4% (-12.9% to 12.5%) larger than the corresponding *piControl* simulations. Only 6 out of 25 models produce a reduction in explained variance, in which MIROC-ESM presents the largest reduction by -12.9%, even larger than that in the *lgm* simulation at -4.7% as compared to the *piControl*. The NAO amplitude

290 in the *abrupt4xCO2* experiment is 2.28 hPa on average (ranging from 1.12 to 3.00 Pa). Though it is 0.11 hPa higher than the corresponding *piControl*, the median of *abrupt4xCO2* NAO amplitude is slightly lower than that of the corresponding *piControl*

(Figure 5. Overall, the NAO is sensitive to GHG forcing and temperature change, as the cooling weakens the NAO and the warming strengthens it, which implies that GHG changes in the future might play a role in modulating NAO behaviour.

The NAO is a variation in the atmospheric pressure differences between the Icelandic Low and the Azores High. As described in Sect. 1, the NAO variability is primarily driven by the internal variability of mid-latitude atmospheric dynamics (Lorenz and Hartmann, 2003). The findings of Rind et al. (2005a, b) show that tropospheric and stratospheric climate changes influence the NAO response via altering propagating waves and angular momentum transport and changes in planetary wave energy. SST (Mosedale et al., 2006; Hurrell et al., 2004), GHG forcing (Stephenson et al., 2006; Barnes and Polvani, 2013), sea ice (Pedersen et al., 2016; Smith et al., 2017) and snow cover changes (Henderson et al., 2018; Spencer and Essery, 2016) could also be potential drivers. Rind et al. (2005b) stated that the AO response during the Ice Age was dominated by changes in the eddy transport of sensible heat and local high-latitude forcing. Lü et al. (2010) examined the drivers of the NAO variability in the PMIP2 *midHolocene* and *lgm* experiments and found that the upward-propagating stationary Rossby waves might lead to NAO amplitude weakening. Based on four simulations, their *midHolocene* experiment presented a slight reduction in the AO intensity. Our results show the opposite change as the NAO amplitude is slightly strengthened, but it is affected by a few models that produce a large enhancement. Our results of the *lgm* and *abrupt4xCO2* experiments agree with the findings of Rind et al. (2005a, b) as the NAO changes positively in global warming experiments and changes negatively in cooling experiments. They stated that the NAO index change is related to the eddy angular momentum transport change. The weakened *lgm* NAO amplitude is possibly due to cooler SST and reduced atmospheric moisture content as well as a shift of stationary waves and a weakened polar vortex linked to wave-mean flow interaction, and thus a reduction in polar westerlies (Lü et al., 2010).

6   Remote effects

A positive NAO in the *piControl* is associated with warmer and wetter northern Europe and central North America and colder and drier Mediterranean and northern North America (Figure 1j, l). Compared with the *piControl*, the *midHolocene* experiment shows a warmer continent associated with the NAO (Figure 6a), with the warming extending farther into central Eurasia and central North America (not shown). Differently, the *lig127k* shows cooling over northern North America and central Europe than the *piControl* (Figure 6c). The DJF mean precipitation associated with the NAO increases over the North Atlantic Ocean north of 30°N and over northern Europe, while decreases over central Europe and North America in the *midHolocene* (Figure 7a). The *lig127k* experiment shows a similar pattern but with less precipitation over east of 20°W and north of 50°N relative to the *piControl* (Figure 7c) However, mean changes in the DJF mean temperature and precipitation associated with the NAO are not robust in the *midHolocene* and *lig127k* as compared to the *piControl*, and the changes are not consistent across the ensembles (Figure 6a-d and 7a-d). The mid-Holocene models capture changes in the mean state (Fig. 2a) that project onto the positive phase of the NAO (Fig. 1h), as reconstructed by Funder et al. (2011). Proxy reconstructions also suggest that regional temperature patterns over Europe were primarily forced by a positive NAO-like phase during the mid-Holocene as opposed to radiative responses forced by changes in the seasonal insolation cycle (Rimbu et al., 2003; Mauri et al., 2014). However, none

of these papers include archives with sufficiently high temporal resolution to compare with the inter-annual variability being
325 investigated here.

The temperature and precipitation patterns associated with the NAO shift southward in the *lgm* experiment (Figures 6e and
7e), which suggests a weakness of features of the positive boreal winter NAO. Associated with the NAO, the *lgm* experiment
presents colder and drier central North America and northern Europe and warmer and wetter Mediterranean and northern North
America in the *lgm* than the *piControl*, with the patterns extending to central continents (not shown). As the strengthened
330 precipitation teleconnection pattern over the western Iberian Peninsula is also present in the mean-state change (Figure 2h),
it suggests that the strengthened Mediterranean precipitation pattern is not necessarily directly forced by the NAO. In the
abrupt4xCO2 experiment, opposite to the *lgm*, features of the positive boreal winter NAO are enhanced than the *piControl*
(Figures 6g and 7g). The associated changes in temperature and precipitation do not match the pattern and magnitude of robust
change in mean state temperature and precipitation (Figure 2), which implies that changes less influence change in mean state
335 climatology in the NAO and have other attributions. For example, the large ice sheets during the LGM limited turbulent air-sea
heat fluxes in the high-latitude North Atlantic that influenced the NAO and cooled the temperature (Sect. 4). The warming in
the *abrupt4xCO2* can be explained by the thermodynamic processes affecting heat and moisture transport without changing the
large-scale atmospheric circulation patterns (Stephenson et al., 2006). The enhanced warming of the surface boundary layer
enhances vertical latent heating, which in turn influences the atmospheric moisture content and baroclinic stability (Lorenz and
340 DeWeaver, 2007).

NAO greatly impacts the European climate (Sect. 1). Figure 8 shows the relationships between the changes in NAO amplitude
and changes in DJF mean precipitation and surface temperature over northern Europe, central Europe, and the Mediterranean
relative to the *piControl*. The change in NAO amplitude is found to have positive correlations with the change in DJF mean
precipitation over northern and central Europe (Figure 8a, b) and a negative correlation over the Mediterranean (Figure 8c).
345 There is no clear relationship between the change in NAO amplitude and the temperature change (Figure 8d to f). The *lgm*
experiment displays a weakened NAO amplitude along with colder mean temperatures, and the *abrupt4xCO2* experiment shows
enhanced NAO amplitude and warmer temperature conversely. The European temperature change overall displays a positive
correlation with the change in the NAO amplitude (Figure 8d to f). Both the pattern and amplitude of the NAO weaken in the
cold *lgm* experiment and strengthen in the warm *abrupt4xCO2* experiment. It suggests that the NAO is sensitive to change in
350 the mean state. Terrestrial proxy data suggest a warmer winter in Europe during the mid-Holocene (Bartlein et al., 2011) and
the last interglacial (Brewer et al., 2008). However, models do not capture this warming in Europe in both experiments and even
present a uniform cooling in the *lig127k*. Mauri et al. (2014) suggest that models fail to capture the full extent of high-latitude
warming over Northern Europe and underestimate the cold Mediterranean temperatures, because they do not capture a positive
NAO-like pattern. This might indicate that the changes in climatological sea level pressure (Fig. 2a) are underestimated in the
355 ensemble.

Earlier studies have noticed a teleconnection existing between ENSO and NAO (Geng et al., 2024; Toniazzo and Scaife,
2006; Hardiman et al., 2019; Zhang et al., 2015; Joshi et al., 2021), though it remains controversial with large uncertainty
(López-Parages et al., 2015; Zhang et al., 2019). The ENSO signals reach the North Atlantic region via the stratosphere

11

(Ineson and Scaife, 2009) and tropospheric pathways (Jiménez-Esteve and Domeisen, 2018). Here we investigate whether a weakened/strengthened ENSO could remotely influence the NAO amplitude. The NAO-ENSO relationship responds nonlinearly to changes in ENSO strength (Hardiman et al., 2019). Enhanced ENSO events affect NAO variability by exciting Rossby waves reaching the North Atlantic through strengthened convection anomalies in the Gulf of Mexico and the Caribbean Sea (Ayarzagüena et al., 2018) and in the tropical Indian and Pacific Ocean (Abid et al., 2021; Joshi et al., 2021). Here, we examine the relationship between change in the strength of ENSO, measured as the standard deviation of nino3.4 index, and change in NAO amplitude (Figure 9). Consistent with Brown et al. (2020), ENSO strengths in the two orbital-forced experiments are weakened (more obviously in the *lig127k* experiment), while they are ambiguous in the *lgm* and *abrupt4xCO2* Figure 9. In contrast, the NAO amplitude weakens in the *lgm* and its changes are ambiguous in the *abrupt4xCO2*, *midHolocene* and *lig127k* experiments (Figure 9). There is no clear relationship between the amplitude changes of ENSO and NAO (Figure 9). It implies that changes in ENSO strength do not remotely influence the NAO amplitude and, therefore, suggest a more nuanced teleconnection then posited by earlier studies.

7   Conclusions

We assessed changes in NAO amplitude and teleconnections in a combination of CMIP5 and CMIP6 models. The simulations for past climates include two altered orbital configurations at the mid-Holocene (*midHolocene*) and LIG (*lig127k*) and a colder-than-present LGM (*lgm*), and one for the future as an idealised warming projection of abrupt quadrupling of CO_2 (*abrupt4xCO2*). The *lgm* and *abrupt4xCO2* are analysed for NAO response to CO_2 forcing. For model evaluation, we compared the *piControl* simulation with the C20 Reanalysis dataset (Compo et al., 2011), as shown in Sect. 3. The *piControl* ensemble reproduces the observed mean state but with biases. The patterns of the positive phase of the NAO and associated teleconnections are consistent between observation and the *piControl* but with variations across the simulations. We explored changes in NAO spatial patterns and explained variance and amplitude. Our results suggest that the NAO change is sensitive to GHG-forcing-induced temperature change but not the orbital configurations. NAO weakens in response to cooling and strengthens to warming. Some of our results are inconsistent with earlier studies, but the inconsistencies are likely affected by the outputs of a few models. The underlying mechanisms are unclear, but previous have highlighted the influence of tropospheric and stratospheric climate changes on NAO behaviour (Rind et al., 2005a, b; Lü et al., 2010). We also discussed changes in NAO teleconnections. The simulated spatial teleconnection patterns associated with the NAO are generally consistent with the theory (see Sect. 1) and are sensitive to the change in NAO amplitude. The *midHolocene* and *lig127k* experiments do not show a clear change in temperature and precipitation associated with the NAO. The weakened NAO in the *lgm* is associated with a cooler and drier northern Europe, while the enhanced NAO in the *abrupt4xCO2* causes a warmer and wetter northern Europe as compared to the *piControl*. We did not find the ENSO-NAO teleconnection suggested by other studies. Further work is required to fully understand the underlying mechanisms driving the NAO change and the associated teleconnections.

390 *Code and data availability.* The processed data for figures are available at https://github.com/annizhao1994/PMIP_NAO and https://doi.org/10.5281/zenodo.15624480.

Author contributions. A.Z. and C.B. performed the bulk of the writing and analysis. A.V. put a large effort into the early stage of the analysis. X.S. contributed to the lgm analysis and revised this manuscript. Y.H. revised the manuscript.

Competing interests. The authors declare that none of the authors has any competing interests.

References

Abe-Ouchi, A., Saito, F., Kageyama, M., Braconnot, P., Harrison, S. P., Lambeck, K., Otto-Bliesner, B. L., Peltier, W. R., Tarasov, L., Peterschmitt, J.-Y., and Takahashi, K.: Ice-sheet configuration in the CMIP5/PMIP3 Last Glacial Maximum experiments, Geoscientific Model Development, 8, 3621–3637, https://doi.org/10.5194/gmd-8-3621-2015, 2015.

Abid, M. A., Kucharski, F., Molteni, F., Kang, I.-S., Tompkins, A. M., and Almazroui, M.: Separating the Indian and Pacific Ocean Impacts on the Euro-Atlantic Response to ENSO and Its Transition from Early to Late Winter, Journal of Climate, 34, 1531–1548, https://doi.org/https://doi.org/10.1175/JCLI-D-20-0075.1, 2021.

Ackerley, D., Reeves, J., Barr, C., Bostock, H., Fitzsimmons, K., Fletcher, M.-S., Gouramanis, C., McGregor, H., Mooney, S., Phipps, S. J., Tibby, J., and Tyler, J.: Evaluation of PMIP2 and PMIP3 simulations of mid-Holocene climate in the Indo-Pacific, Australasian and Southern Ocean regions, Climate of the Past, 13, 1661–1684, https://doi.org/10.5194/cp-13-1661-2017, 2017.

Ambaum, M. H. P., Hoskins, B. J., and Stephenson, D. B.: Arctic Oscillation or North Atlantic Oscillation?, Journal of Climate, 14, 3495 – 3507, https://doi.org/https://doi.org/10.1175/1520-0442(2001)014<3495:AOONAO>2.0.CO;2, 2001.

Argus, D. F., Peltier, W. R., Drummond, R., and Moore, A. W.: The Antarctica component of postglacial rebound model ICE-6G_C (VM5a) based on GPS positioning, exposure age dating of ice thicknesses, and relative sea level histories, Geophysical Journal International, 198, 537–563, https://doi.org/10.1093/gji/ggu140, 2014.

Ayarzagüena, B., Ineson, S., Dunstone, N. J., Baldwin, M. P., and Scaife, A. A.: Intraseasonal Effects of El Niño–Southern Oscillation on North Atlantic Climate, Journal of Climate, 31, 8861–8873, https://doi.org/https://doi.org/10.1175/JCLI-D-18-0097.1, 2018.

Bader, J., Mesquita, M. D. S., Hodges, K. I., Keenlyside, N., Østerhus, S., and Miles, M.: A review on Northern Hemisphere sea-ice, storminess and the North Atlantic Oscillation: Observations and projected changes, Atmospheric Research, 101, 809–834, https://doi.org/https://doi.org/10.1016/j.atmosres.2011.04.007, 2011.

Balaji, V., Taylor, K. E., Juckes, M., Lawrence, B. N., Durack, P. J., Lautenschlager, M., Blanton, C., Cinquini, L., Denvil, S., Elkington, M., Guglielmo, F., Guilyardi, E., Hassell, D., Kharin, S., Kindermann, S., Nikonov, S., Radhakrishnan, A., Stockhause, M., Weigel, T., and Williams, D.: Requirements for a global data infrastructure in support of CMIP6, Geoscientific Model Development, 11, 3659–3680, https://doi.org/10.5194/gmd-11-3659-2018, 2018.

Bao, Q., Lin, P., Zhou, T., Liu, Y., Yu, Y., Wu, G., He, B., He, J., Li, L., Li, J., Li, C., Liu, H., Qiao, F., Song, Z., Wang, B., Wang, J., Wang, P., Wang, X., Wang, Z., Wu, B., Wu, T., Xu, Y., Yu, H., Zhao, W., Zheng, W., and Zhou, L.: The flexible global ocean-atmosphere-land system model, spectral version 2: FGOALS-s2, Advances in Atmospheric Sciences, 30, 561–576, https://doi.org/10.1007/s00376-012-2113-9, 2013.

Barlow, N. L. M., McClymont, E. L., Whitehouse, P. L., Stokes, C. R., Jamieson, S. S. R., Woodroffe, S. A., Bentley, M. J., Callard, S. L., Cofaigh, C. Ó., Evans, D. J. A., Horrocks, J. R., Lloyd, J. M., Long, A. J., Margold, M., Roberts, D. H., and Sanchez-Montes, M. L.: Lack of evidence for a substantial sea-level fluctuation within the Last Interglacial, Nature Geoscience, 11, 627–634, https://doi.org/10.1038/s41561-018-0195-4, 2018.

Barnes, E. A. and Polvani, L.: Response of the Midlatitude Jets, and of Their Variability, to Increased Greenhouse Gases in the CMIP5 Models, Journal of Climate, 26, 7117–7135, https://doi.org/https://doi.org/10.1175/JCLI-D-12-00536.1, 2013.

Bartlein, P. J. and Shafer, S. L.: Paleo calendar-effect adjustments in time-slice and transient climate-model simulations (PaleoCalAdjust v1.0): impact and strategies for data analysis, Geoscientific Model Development, 12, 3889–3913, https://doi.org/10.5194/gmd-12-3889-2019, 2019.

Bartlein, P. J., Harrison, S., Brewer, S., Connor, S., Davis, B., Gajewski, K., Guiot, J., Harrison-Prentice, T., Henderson, A., and Peyron, O.: Pollen-based continental climate reconstructions at 6 and 21 ka: a global synthesis, Climate Dynamics, 37, 775–802, https://doi.org/10.1007/s00382-010-0904-1, 2011.

440   Berger, A.: Long-term variations of caloric insolation resulting from the earth's orbital elements, Quaternary Res., 9, 139–167, 1978.

Berger, A. and Loutre, M.-F.: Insolation values for the climate of the last 10 million years, Quaternary Science Reviews, 10, 297–317, 1991.

Boucher, O., Servonnat, J., Albright, A. L., Aumont, O., Balkanski, Y., Bastrikov, V., Bekki, S., Bonnet, R., Bony, S., Bopp, L., Braconnot, P., Brockmann, P., Cadule, P., Caubel, A., Cheruy, F., Codron, F., Cozic, A., Cugnet, D., D'Andrea, F., Davini, P., Lavergne, C., Denvil, S., Deshayes, J., Devilliers, M., Ducharne, A., Dufresne, J., Dupont, E., Éthé, C., Fairhead, L., Falletti, L., Flavoni, S., Foujols, M., Gardoll,
445   S., Gastineau, G., Ghattas, J., Grandpeix, J., Guenet, B., Guez, Lionel, E., Guilyardi, E., Guimberteau, M., Hauglustaine, D., Hourdin, F., Idelkadi, A., Joussaume, S., Kageyama, M., Khodri, M., Krinner, G., Lebas, N., Levavasseur, G., Lévy, C., Li, L., Lott, F., Lurton, T., Luyssaert, S., Madec, G., Madeleine, J., Maignan, F., Marchand, M., Marti, O., Mellul, L., Meurdesoif, Y., Mignot, J., Musat, I., Ottlé, C., Peylin, P., Planton, Y., Polcher, J., Rio, C., Rochetin, N., Rousset, C., Sepulchre, P., Sima, A., Swingedouw, D., Thiéblemont, R., Traore, A. K., Vancoppenolle, M., Vial, J., Vialard, J., Viovy, N., and Vuichard, N.: Presentation and Evaluation of the IPSL-CM6A-LR Climate
450   Model, Journal of Advances in Modeling Earth Systems, 12, p.e2019MS002 010–n/a, https://doi.org/10.1029/2019MS002010, 2020.

Braconnot, P., Joussaume, S., de Noblet, N., and Ramstein, G.: Mid-Holocene and Last Glacial Maximum African monsoon changes as simulated within the Paleoclimate Modelling Intercomparison Project, Global and planetary change, 26, 51–66, 2000.

Braconnot, P., Otto-Bliesner, B., Harrison, S., Joussaume, S., Peterchmitt, J.-Y., Abe-Ouchi, A., Crucifix, M., Driesschaert, E., Fichefet, T., Hewitt, C. D., Kageyama, M., Kitoh, A., La\^\iné, A., Loutre, M.-F., Marti, O., Merkel, U., Ramstein, G., Valdes, P., Weber, S. L.,
455   Yu, Y., and Zhao, Y.: Results of PMIP2 coupled simulations of the Mid-Holocene and Last Glacial Maximum – Part 1: experiments and large-scale features, Climate of the Past, 3, 261–277, https://doi.org/10.5194/cp-3-261-2007, 2007.

Brewer, S., Guiot, J., Sánchez-Goñi, M. F., and Klotz, S.: The climate in Europe during the Eemian: a multi-method approach using pollen data, Quaternary Science Reviews, 27, 2303–2315, https://doi.org/10.1016/j.quascirev.2008.08.029, 2008.

Brierley, C. and Wainer, I.: Inter-annual variability in the tropical Atlantic from the Last Glacial Maximum into future climate projections
460   simulated by CMIP5/PMIP3, Climate of the Past, 14, 1377–1390, https://doi.org/10.5194/cp-14-1377-2018, 2018.

Brierley, C., Thirumalai, K., Grindrod, E., and Barnsley, J.: Indian Ocean variability changes in the Paleoclimate Modelling Intercomparison Project, Climate of the Past, 19, 681–701, https://doi.org/10.5194/cp-19-681-2023, 2023.

Brierley, C. M., Zhao, A., Harrison, S. P., Braconnot, P., Williams, C. J. R., Thornalley, D. J. R., Shi, X., Peterschmitt, J.-Y., Ohgaito, R., Kaufman, D. S., Kageyama, M., Hargreaves, J. C., Erb, M. P., Emile-Geay, J., D'Agostino, R., Chandan, D., Carré, M., Bartlein,
465   P. J., Zheng, W., Zhang, Z., Zhang, Q., Yang, H., Volodin, E. M., Tomas, R. A., Routson, C., Peltier, W. R., Otto-Bliesner, B., Morozova, P. A., McKay, N. P., Lohmann, G., Legrande, A. N., Guo, C., Cao, J., Brady, E., Annan, J. D., and Abe-Ouchi, A.: Large-scale features and evaluation of the PMIP4-CMIP6 *midHolocene* simulations, Climate of the Past, 16, 1847–1872, https://doi.org/10.5194/cp-16-1847-2020, 2020.

Brown, J. R., Brierley, C. M., An, S.-I., Guarino, M.-V., Stevenson, S., Williams, C. J. R., Zhang, Q., Zhao, A., Abe-Ouchi, A., Braconnot,
470   P., Brady, E. C., Chandan, D., D'Agostino, R., Guo, C., LeGrande, A. N., Lohmann, G., Morozova, P. A., Ohgaito, R., O'ishi, R., Otto-Bliesner, B. L., Peltier, W. R., Shi, X., Sime, L., Volodin, E. M., Zhang, Z., and Zheng, W.: Comparison of past and future simulations of ENSO in CMIP5/PMIP3 and CMIP6/PMIP4 models, Climate of the Past, 16, 1777–1805, https://doi.org/10.5194/cp-16-1777-2020, 2020.

Cao, J., Wang, B., Yang, Y.-M., Ma, L., Li, J., Sun, B., Bao, Y., He, J., Zhou, X., and Wu, L.: The NUIST Earth System Model (NESM) version
475   3: description and preliminary evaluation, Geoscientific Model Development, 11, 2975–2993, https://doi.org/10.5194/gmd-11-2975-2018,
       2018.

Chandan, D. and Peltier, W. R.: Regional and global climate for the mid-Pliocene using the University of Toronto version of CCSM4 and
       PlioMIP2 boundary conditions, Climate of the Past, 13, 919–942, https://doi.org/10.5194/cp-13-919-2017, 2017.

Clark, P. U. and Mix, A. C.: Ice sheets and sea level of the Last Glacial Maximum, Quaternary Science Reviews, 21, 1–7,
480   https://doi.org/https://doi.org/10.1016/S0277-3791(01)00118-4, 2002.

Clark, P. U., Dyke, A. S., Shakun, J. D., Carlson, A. E., Clark, J., Wohlfarth, B., Mitrovica, J. X., Hostetler, S. W., and McCabe, A. M.: The
       Last Glacial Maximum, Science, 325, 710–714, https://doi.org/10.1126/science.1172873, 2009.

Collins, W., Bellouin, N., Doutriaux-Boucher, M., Gedney, N., Halloran, P., Hinton, T., Hughes, J., Jones, C., Joshi, M., Liddicoat,
       S., et al.: Development and evaluation of an Earth-System model–HadGEM2, Geoscientific Model Development, 4, 1051–1075,
485   https://doi.org/10.5194/gmd-4-1051-2011, 2011.

Compo, G. P., Whitaker, J. S., Sardeshmukh, P. D., Matsui, N., Allan, R. J., Yin, X., Gleason, B. E., Vose, R. S., Rutledge, G., Bessemoulin,
       P., Brönnimann, S., Brunet, M., Crouthamel, R. I., Grant, A. N., Groisman, P. Y., Jones, P. D., Kruk, M. C., Kruger, A. C., Marshall, G. J.,
       Maugeri, M., Mok, H. Y., Nordli, Ø., Ross, T. F., Trigo, R. M., Wang, X. L., Woodruff, S. D., and Worley, S. J.: The twentieth century
       reanalysis project, Quarterly Journal of the Royal Meteorological Society, 137, 1–28, https://doi.org/10.1002/qj.776, 2011.

490   Cook, E. R., Kushnir, Y., Smerdon, J. E., Williams, A. P., Anchukaitis, K. J., and Wahl, E. R.: A Euro-Mediterranean tree-ring reconstruction
       of the winter NAO index since 910 C.E., Climate Dynamics, 53, 1567–1580, https://doi.org/10.1007/s00382-019-04696-2, 2019.

Cornes, R. C., Jones, P. D., Briffa, K. R., and Osborn, T. J.: Estimates of the North Atlantic Oscillation back to 1692 using a Paris–London
       westerly index, International Journal of Climatology, 33, 228–248, https://doi.org/https://doi.org/10.1002/joc.3416, 2013.

Craig, A., Valcke, S., and Coquart, L.: Development and performance of a new version of the OASIS coupler, OASIS3-MCT-3.0, Geoscien-
495   tific Model Development, 10, 3297–3308, https://doi.org/10.5194/gmd-10-3297-2017, 2017.

Döscher, R., Acosta, M., Alessandri, A., Anthoni, P., Arneth, A., Arsouze, T., Bergmann, T., Bernadello, R., Bousetta, S., Caron, L.-P.,
       Carver, G., Castrillo, M., Catalano, F., Cvijanovic, I., Davini, P., Dekker, E., Doblas-Reyes, F. J., Docquier, D., Echevarria, P., Fladrich, U.,
       Fuentes-Franco, R., Gröger, M., v. Hardenberg, J., Hieronymus, J., Karami, M. P., Keskinen, J.-P., Koenigk, T., Makkonen, R., Massonnet,
       F., Ménégoz, M., Miller, P. A., Moreno-Chamarro, E., Nieradzik, L., van Noije, T., Nolan, P., O'Donnell, D., Ollinaho, P., van den Oord,
500   G., Ortega, P., Prims, O. T., Ramos, A., Reerink, T., Rousset, C., Ruprich-Robert, Y., Le Sager, P., Schmith, T., Schrödner, R., Serva, F.,
       Sicardi, V., Sloth Madsen, M., Smith, B., Tian, T., Tourigny, E., Uotila, P., Vancoppenolle, M., Wang, S., Wårlind, D., Willén, U., Wyser,
       K., Yang, S., Yepes-Arbós, X., and Zhang, Q.: The EC-Earth3 Earth System Model for the Climate Model Intercomparison Project 6,
       Geoscientific Model Development Discussions, 2021, 1–90, https://doi.org/10.5194/gmd-2020-446, 2021.

Dufresne, J.-L., Foujols, M.-A., Denvil, S., Caubel, A., Marti, O., Aumont, O., Balkanski, Y., Bekki, S., Bellenger, H., Benshila, R., Bony,
505   S., Bopp, L., Braconnot, P., Brockmann, P., Cadule, P., Cheruy, F., Codron, F., Cozic, A., Cugnet, D., de Noblet, N., Duvel, J.-P., Ethé, C.,
       Fairhead, L., Fichefet, T., Flavoni, S., Friedlingstein, P., Grandpeix, J.-Y., Guez, L., Guilyardi, E., Hauglustaine, D., Hourdin, F., Idelkadi,
       A., Ghattas, J., Joussaume, S., Kageyama, M., Krinner, G., Labetoulle, S., Lahellec, A., Lefebvre, M.-P., Lefevre, F., Levy, C., Li, Z. X.,
       Lloyd, J., Lott, F., Madec, G., Mancip, M., Marchand, M., Masson, S., Meurdesoif, Y., Mignot, J., Musat, I., Parouty, S., Polcher, J., Rio,
       C., Schulz, M., Swingedouw, D., Szopa, S., Talandier, C., Terray, P., Viovy, N., and Vuichard, N.: Climate change projections using the
510   IPSL-CM5 Earth System Model: from CMIP3 to CMIP5, Climate Dynamics, 40, 2123–2165, https://doi.org/10.1007/s00382-012-1636-1,
       2013.

Eyring, V., Bony, S., Meehl, G. A., Senior, C. A., Stevens, B., Stouffer, R. J., and Taylor, K. E.: Overview of the Coupled Model
Intercomparison Project Phase 6 (CMIP6) experimental design and organization, Geoscientific Model Development, 9, 1937–1958,
https://doi.org/10.5194/gmd-9-1937-2016, 2016.

515 Feldstein, S. B. and Franzke, C. L. E.: Atmospheric Teleconnection Patterns, pp. 54–104, Cambridge University Press, Cambridge,
https://doi.org/DOI: 10.1017/9781316339251.004, 2017.

Flato, G., Marotzke, J., Abiodun, B., Braconnot, P., Chou, S. C., Collins, W., Cox, P., Driouech, F., Emori, S., Eyring, V., Forest, C., Gleckler,
P., Guilyardi, E., Jakob, C., Kattsov, V., Reason, C., Rummukainen, M., AchutaRao, K., Anav, A., Andrews, T., Baehr, J., Bindoff, N. L.,
Bodas-Salcedo, A., Catto, J., Chambers, D., Chang, P., Dai, A., Deser, C., Doblas-Reyes, F., Durack, P. J., Eby, M., de Elia, R., Fichefet, T.,
520 Forster, P., Frame, D., Fyfe, J., Gbobaniyi, E., Gillett, N., González-Rouco, J. F., Goodess, C., Griffies, S., Hall, A., Harrison, S., Hense, A.,
Hunke, E., Ilyina, T., Ivanova, D., Johnson, G., Kageyama, M., Kharin, V., Klein, S. A., Knight, J., Knutti, R., Landerer, F., Lee, T., Li, H.,
Mahowald, N., Mears, C., Meehl, G., Morice, C., Msadek, R., Myhre, G., Neelin, J. D., Painter, J., Pavlova, T., Perlwitz, J., Peterschmitt,
J.-Y., Räisänen, J., Rauser, F., Reid, J., Rodwell, M., Santer, B., Scaife, A. A., Schulz, J., Scinocca, J., Sexton, D., Shindell, D., Shiogama,
H., Sillmann, J., Simmons, A., Sperber, K., Stephenson, D., Stevens, B., Stott, P., Sutton, R., Thorne, P. W., van Oldenborgh, G. J., Vecchi,
525 G., Webb, M., Williams, K., Woollings, T., Xie, S.-P., and Zhang, J.: Evaluation of climate models, in: Climate change 2013: the physical
science basis. Contribution of Working Group I to the Fifth Assessment Report of the Intergovernmental Panel on Climate Change, edited
by Stocker, T., Qin, D., Plattner, G.-K., Tignor, M., Allen, S., Boschung, J., Nauels, A., Xia, Y., Bex, V., and Midgley, P., pp. 741–866,
Cambridge University Press, 2013.

Funder, S., Goosse, H., Jepsen, H., Kaas, E., Kjær, K. H., Korsgaard, N. J., Larsen, N. K., Linderson, H., Lyså, A., Möller, P., Olsen,
530 J., and Willerslev, E.: A 10,000-Year Record of Arctic Ocean Sea-Ice Variability—View from the Beach, Science, 333, 747–750, http:
//www.jstor.org/stable/27978395, 2011.

Geng, X., Kug, J.-S., and Kosaka, Y.: Future changes in the wintertime ENSO-NAO teleconnection under greenhouse warming, npj Climate
and Atmospheric Science, 7, 81, https://doi.org/10.1038/s41612-024-00627-z, 2024.

Gent, P. R., Danabasoglu, G., Donner, L. J., Holland, M. M., Hunke, E. C., Jayne, S. R., Lawrence, D. M., Neale, R. B., Rasch, P. J.,
535 Vertenstein, M., Worley, P. H., Yang, Z.-L., and Zhang, M.: The community climate system model version 4, Journal of Climate, 24,
4973–4991, https://doi.org/10.1175/2011JCLI4083.1, 2011.

Gettelman, A., Hannay, C., Bacmeister, J. T., Neale, R. B., Pendergrass, A. G., Danabasoglu, G., Lamarque, J., Fasullo, J. T., Bailey, D. A.,
Lawrence, D. M., and Mills, M. J.: High Climate Sensitivity in the Community Earth System Model Version 2 (CESM2), Geophysical
Research Letters, 46, 8329–8337, https://doi.org/10.1029/2019GL083978, 2019.

540 Giorgetta, M. A., Jungclaus, J., Reick, C. H., Legutke, S., Bader, J., Böttinger, M., Brovkin, V., Crueger, T., Esch, M., Fieg, K., Glushak,
K., Gayler, V., Haak, H., Hollweg, H.-D., Ilyina, T., Kinne, S., Kornblueh, L., Matei, D., Mauritsen, T., Mikolajewicz, U., Mueller, W.,
Notz, D., Pithan, F., Raddatz, T., Rast, S., Redler, R., Roeckner, E., Schmidt, H., Schnur, R., Segschneider, J., Six, K. D., Stockhause, M.,
Timmreck, C., Wegner, J., Widmann, H., Wieners, K.-H., Claussen, M., Marotzke, J., and Stevens, B.: Climate and carbon cycle changes
from 1850 to 2100 in MPI-ESM simulations for the Coupled Model Intercomparison Project phase 5, Journal of Advances in Modeling
545 Earth Systems, 5, 572–597, https://doi.org/10.1002/jame.20038, 2013.

Gladstone, R. M., Ross, I., Valdes, P. J., Abe-Ouchi, A., Braconnot, P., Brewer, S., Kageyama, M., Kitoh, A., Legrande, A., Marti, O.,
Ohgaito, R., Otto-Bliesner, B., Peltier, W. R., and Vettoretti, G.: Mid-Holocene NAO: A PMIP2 model intercomparison, Geophysical
Research Letters, 32, https://doi.org/https://doi.org/10.1029/2005GL023596, 2005.

Govin, A., Braconnot, P., Capron, E., Cortijo, E., Duplessy, J.-C., Jansen, E., Labeyrie, L., Landais, A., Marti, O., Michel, E., Mosquet, E., Risebrobakken, B., Swingedouw, D., and Waelbroeck, C.: Persistent influence of ice sheet melting on high northern latitude climate during the early Last Interglacial, Climate of the Past, 8, 483–507, https://doi.org/10.5194/cp-8-483-2012, 2012.

Gulev, S. K., Thorne, P., Ahn, J., Dentener, F., Domingues, C., Gerland, S., Gong, D., Kaufman, D., Nnamchi, H., Quaas, J., Rivera, J., Sathyendranath, S., Smith, S., Trewin, B., von Shuckmann, K., and Vose, R.: Changing State of the Climate System, in: Climate Change 2021: The Physical Science Basis. Contribution of Working Group I to the Sixth Assessment Report of the Intergovernmental Panel on Climate Change, edited by Masson-Delmotte, V., Zhai, P., Pirani, A., Connors, S. L., Péan, C., Berger, S., Caud, N., Chen, Y., Goldfarb, L., Gomis, M. I., Huang, M., Leitzell, K., Lonnoy, E., Matthews, J., Maycock, T. K., Waterfield, T., Yelekçi, O., Yu, R., , and Zhou, B., Cambridge University Press, Cambridge, United Kingdom and New York, U.S.A., 2021.

Guo, C., Bentsen, M., Bethke, I., Ilicak, M., Tjiputra, J., Toniazzo, T., Schwinger, J., and Otterå, O. H.: Description and evaluation of NorESM1-F: a fast version of the Norwegian Earth System Model (NorESM), Geoscientific Model Development, 12, 343–362, https://doi.org/10.5194/gmd-12-343-2019, 2019.

Găinuşă-Bogdan, A., Swingedouw, D., Yiou, P., Cattiaux, J., Codron, F., and Michel, S.: AMOC and summer sea ice as key drivers of the spread in mid-holocene winter temperature patterns over Europe in PMIP3 models, Global and Planetary Change, 184, 103 055, https://doi.org/10.1016/j.gloplacha.2019.103055, 2020.

Hajima, T., Watanabe, M., Yamamoto, A., Tatebe, H., Noguchi, M. A., Abe, M., Ohgaito, R., Ito, A., Yamazaki, D., Okajima, H., Ito, A., Takata, K., Ogochi, K., Watanabe, S., and Kawamiya, M.: Description of the MIROC-ES2L Earth system model and evaluation of its climate–biogeochemical processes and feedbacks, Geoscientific Model Development, 13, 2197–2244, https://doi.org/10.5194/gmd-13-2197-2020, 2020.

Hall, R. J., Mitchell, D. M., Seviour, W. J. M., and Wright, C. J.: Persistent Model Biases in the CMIP6 Representation of Stratospheric Polar Vortex Variability, Journal of Geophysical Research: Atmospheres, 126, e2021JD034 759, https://doi.org/https://doi.org/10.1029/2021JD034759, 2021.

Hardiman, S. C., Dunstone, N. J., Scaife, A. A., Smith, D. M., Ineson, S., Lim, J., and Fereday, D.: The Impact of Strong El Niño and La Niña Events on the North Atlantic, Geophysical Research Letters, 46, 2874–2883, https://doi.org/https://doi.org/10.1029/2018GL081776, 2019.

Harrison, S. P., Bartlein, P., Izumi, K., Li, G., Annan, J., Hargreaves, J., Braconnot, P., and Kageyama, M.: Evaluation of CMIP5 palaeo-simulations to improve climate projections, Nature Climate Change, 5, 735–743, https://doi.org/10.1038/nclimate2649, 2015.

Harvey, B. J., Shaffrey, L. C., and Woollings, T. J.: Equator-to-pole temperature differences and the extra-tropical storm track responses of the CMIP5 climate models, Climate Dynamics, 43, 1171–1182, https://doi.org/10.1007/s00382-013-1883-9, 2014.

Harvey, B. J., Shaffrey, L. C., and Woollings, T. J.: Deconstructing the climate change response of the Northern Hemisphere wintertime storm tracks, Climate Dynamics, 45, 2847–2860, https://doi.org/10.1007/s00382-015-2510-8, 2015.

Hazeleger, W., Wang, X., Severijns, C., Ştefănescu, S., Bintanja, R., Sterl, A., Wyser, K., Semmler, T., Yang, S., Van den Hurk, B., van Noije, T., van der Linden, E., van der Wiel, K Hazeleger, W., Bintanja, R., Hazeleger, W., and Bintanja, R.: EC-Earth V2. 2: description and validation of a new seamless earth system prediction model, Climate dynamics, 39, 2611–2629, https://doi.org/10.1007/s00382-011-1228-5, 2012.

He, B., Yu, Y., Bao, Q., Lin, P., Liu, H., Li, J., Wang, L., Liu, Y., Wu, G., Chen, K., Guo, Y., Zhao, S., Zhang, X., Song, M., and Xie, J.: CAS FGOALS-f3-L Model dataset descriptions for CMIP6 DECK experiments, Atmospheric and Oceanic Science Letters, ahead-of-print, 1–7, https://doi.org/10.1080/16742834.2020.1778419, 2020.

Henderson, G. R., Peings, Y., Furtado, J. C., and Kushner, P. J.: Snow–atmosphere coupling in the Northern Hemisphere, Nature Climate Change, 8, 954–963, https://doi.org/10.1038/s41558-018-0295-6, 2018.

Hernández, A., Martin-Puertas, C., Moffa-Sánchez, P., Moreno-Chamarro, E., Ortega, P., Blockley, S., Cobb, K. M., Comas-Bru, L., Giralt, S., Goosse, H., Luterbacher, J., Martrat, B., Muscheler, R., Parnell, A., Pla-Rabes, S., Sjolte, J., Scaife, A. A., Swingedouw, D., Wise, E., and Xu, G.: Modes of climate variability: Synthesis and review of proxy-based reconstructions through the Holocene, Earth-Science Reviews, 209, 103 286, https://doi.org/https://doi.org/10.1016/j.earscirev.2020.103286, 2020.

Hurrell, J. W.: Decadal Trends in the North Atlantic Oscillation: Regional Temperatures and Precipitation, Science, 269, 676–679, https://doi.org/10.1126/science.269.5224.676, 1995.

Hurrell, J. W., Kushnir, Y., Ottersen, G., and Visbeck, M.: An Overview of the North Atlantic Oscillation, pp. 1–35, American Geophysical Union (AGU), https://doi.org/https://doi.org/10.1029/134GM01, 2003.

Hurrell, J. W., Hoerling, M. P., Phillips, A. S., and Xu, T.: Twentieth century north atlantic climate change. Part I: assessing determinism, Climate Dynamics, 23, 371–389, https://doi.org/10.1007/s00382-004-0432-y, 2004.

Ineson, S. and Scaife, A. A.: The role of the stratosphere in the European climate response to El Niño, Nature Geoscience, 2, 32–36, https://doi.org/10.1038/ngeo381, 2009.

IPCC: Annex II: Models [Gutiérrez, J M., A.-M. Tréguier (eds.)], in: Climate Change 2021: The Physical Science Basis. Contribution of Working Group I to the Sixth Assessment Report of the Intergovernmental Panel on Climate Change, edited by Masson-Delmotte, V., Zhai, P., Pirani, A., Connors, S. L., Péan, C., Berger, S., Caud, N., Chen, Y., Goldfarb, L., Gomis, M. I., Huang, M., Leitzell, K., Lonnoy, E., Matthews, J., Maycock, T. K., Waterfield, T., Yelekçi, O., Yu, R., , and Zhou, B., Cambridge University Press, Cambridge, United Kingdom and New York, U.S.A., https://doi.org/10.1017/9781009157896.016, 2021a.

IPCC: Annex IV: Modes of Variability [Cassou, C., A. Cherchi, Y. Kosaka (eds.)]., in: Climate Change 2021: The Physical Science Basis. Contribution of Working Group I to the Sixth Assessment Report of the Intergovernmental Panel on Climate Change, edited by Masson-Delmotte, V., Zhai, P., Pirani, A., Connors, S. L., Péan, C., Berger, S., Caud, N., Chen, Y., Goldfarb, L., Gomis, M. I., Huang, M., Leitzell, K., Lonnoy, E., Matthews, J., Maycock, T. K., Waterfield, T., Yelekçi, O., Yu, R., , and Zhou, B., Cambridge University Press, Cambridge, United Kingdom and New York, U.S.A., https://doi.org/10.1017/9781009157896.018, 2021b.

Ivanovic, R. F., Gregoire, L. J., Kageyama, M., Roche, D. M., Valdes, P. J., Burke, A., Drummond, R., Peltier, W. R., and Tarasov, L.: Transient climate simulations of the deglaciation 21–9 thousand years before present (version 1) – PMIP4 Core experiment design and boundary conditions, Geoscientific Model Development, 9, 2563–2587, https://doi.org/10.5194/gmd-9-2563-2016, 2016.

Jiménez-Esteve, B. and Domeisen, D. I. V.: The Tropospheric Pathway of the ENSO–North Atlantic Teleconnection, Journal of Climate, 31, 4563–4584, https://doi.org/https://doi.org/10.1175/JCLI-D-17-0716.1, 2018.

Jones, P. D., Jonsson, T., and Wheeler, D.: Extension to the North Atlantic oscillation using early instrumental pressure observations from Gibraltar and south-west Iceland, International Journal of Climatology, 17, 1433–1450, https://doi.org/https://doi.org/10.1002/(SICI)1097-0088(19971115)17:13<1433::AID-JOC203>3.0.CO;2-P, 1997.

Jonkers, L., Laepple, T., Rillo, M. C., Shi, X., Dolman, A. M., Lohmann, G., Paul, A., Mix, A., and Kucera, M.: Strong temperature gradients in the ice age North Atlantic Ocean revealed by plankton biogeography, Nature Geoscience, 16, 1114–1119, https://doi.org/10.1038/s41561-023-01328-7, 2023.

Joshi, M. K., Abid, M. A., and Kucharski, F.: The Role of an Indian Ocean Heating Dipole in the ENSO Teleconnection to the North Atlantic European Region in Early Winter during the Twentieth Century in Reanalysis and CMIP5 Simulations, Journal of Climate, 34, 1047–1060, https://doi.org/https://doi.org/10.1175/JCLI-D-20-0269.1, 2021.

625   Joussaume, S. and Taylor, K. E.: Status of the Paleoclimate Modelling Intercomparison Project (PMIP).Proceedings of the first international
       AMIP scientific conference., pp. 425–430, 1995.

Juckes, M., Taylor, K. E., Durack, P. J., Lawrence, B., Mizielinski, M. S., Pamment, A., Peterschmitt, J.-Y., Rien, M., and Sénési, S.: The
       CMIP6 Data Request (DREQ, version 01.00.31), Geoscientific Model Development, 13, 201–224, https://doi.org/10.5194/gmd-13-201-
       2020, 2020.

630   Kageyama, M., Braconnot, P., Harrison, S. P., Haywood, A. M., Jungclaus, J. H., Otto-Bliesner, B. L., Abe-Ouchi, A., Albani, S., Bartlein,
       P. J., and Brierley, C.: The PMIP4 contribution to CMIP6-Part 1: Overview and over-arching analysis plan, Geoscientific Model Develop-
       ment, 11, 1033–1057, https://doi.org/10.5194/gmd-11-1033-2018, 2018.

Kageyama, M., Harrison, S. P., Kapsch, M.-L., Lofverstrom, M., Lora, J. M., Mikolajewicz, U., Sherriff-Tadano, S., Vadsaria, T., Abe-Ouchi,
       A., Bouttes, N., Chandan, D., Gregoire, L. J., Ivanovic, R. F., Izumi, K., LeGrande, A. N., Lhardy, F., Lohmann, G., Morozova, P. A.,
635   Ohgaito, R., Paul, A., Peltier, W. R., Poulsen, C. J., Quiquet, A., Roche, D. M., Shi, X., Tierney, J. E., Valdes, P. J., Volodin, E., and Zhu,
       J.: The PMIP4 Last Glacial Maximum experiments: preliminary results and comparison with the PMIP3 simulations, Climate of the Past,
       17, 1065–1089, https://doi.org/10.5194/cp-17-1065-2021, 2021.

Kelley, M., Schmidt, G. A., Nazarenko, L., Bauer, S. E., Ruedy, R., Russell, G. L., Ackerman, A. S., Aleinov, I., Bauer, M., Bleck, R.,
       Canuto, V., Cesana, G., Cheng, Y., Clune, T. L., Cook, B. I., Cruz, C. A., Del Genio, A. D., Elsaesser, G. S., Faluvegi, G., Kiang, N. Y.,
640   Kim, D., Lacis, A. A., Leboissetier, A., LeGrande, A. N., Lo, K. K., Marshall, J., Matthews, E. E., McDermid, S., Mezuman, K., Miller,
       R. L., Murray, L. T., Oinas, V., Orbe, C., Pérez García-Pando, C., Perlwitz, J. P., Puma, M. J., Rind, D., Romanou, A., Shindell, D. T.,
       Sun, S., Tausnev, N., Tsigaridis, K., Tselioudis, G., Weng, E., Wu, J., and Yao, M.-S.: GISS-E2.1: Configurations and climatology, J. Adv.
       Model. Earth Syst., 12, e2019MS002 025, https://doi.org/10.1029/2019MS002025, 2020.

Khosravi, N., Wang, Q., Koldunov, N., Hinrichs, C., Semmler, T., Danilov, S., and Jung, T.: The Arctic Ocean in
645   CMIP6 Models: Biases and Projected Changes in Temperature and Salinity, Earth's Future, 10, e2021EF002 282,
       https://doi.org/https://doi.org/10.1029/2021EF002282, 2022.

Kimoto, M., Jin, F.-F., Watanabe, M., and Yasutomi, N.: Zonal—eddy coupling and a neutral mode theory for the Arctic Oscillation, Geo-
       physical Research Letters, 28, 737–740, https://doi.org/https://doi.org/10.1029/2000GL012377, 2001.

Lee, J. Y., Marotzke, J., Bala, G., Cao, L., Corti, S., Dunne, J., Engelbrecht, F., Fischer, E., Fyfe, J., Jones, C., Maycock, A., Mutemi,
650   J., Ndiaye, O., Panickal, S., and Zhou, T.: Future Global Climate: Scenario-Based Projections and Near-Term Information., in: Climate
       Change 2021: The Physical Science Basis. Contribution of Working Group I to the Sixth Assessment Report of the Intergovernmental
       Panel on Climate Change, edited by Masson-Delmotte, V., Zhai, P., Pirani, A., Connors, S. L., Péan, C., Berger, S., Caud, N., Chen, Y.,
       Goldfarb, L., Gomis, M. I., Huang, M., Leitzell, K., Lonnoy, E., Matthews, J., Maycock, T. K., Waterfield, T., Yelekçi, O., Yu, R., , and
       Zhou, B., Cambridge University Press, 2021.

655   Li, L., Lin, P., Yu, Y., Wang, B., Zhou, T., Liu, L., Liu, J., Bao, Q., Xu, S., Huang, W., Xia, K., Pu, Y., Dong, L., Shen, S., Liu, Y., Hu, N.,
       Liu, M., Sun, W., Shi, X., Zheng, W., Wu, B., Song, M., Liu, H., Zhang, X., Wu, G., Xue, W., Huang, X., Yang, G., Song, Z., and Qiao,
       F.: The flexible global ocean-atmosphere-land system model, Grid-point Version 2: FGOALS-g2, Advances in Atmospheric Sciences, 30,
       543–560, https://doi.org/10.1007/s00376-012-2140-6, 2013.

Li, L., Yu, Y., Tang, Y., Lin, P., Xie, J., Song, M., Dong, L., Zhou, T., Liu, L., Wang, L., Pu, Y., Chen, X., Chen, L., Xie, Z., Liu, H., Zhang,
660   L., Huang, X., Feng, T., Zheng, W., Xia, K., Liu, H., Liu, J., Wang, Y., Wang, L., Jia, B., Xie, F., Wang, B., Zhao, S., Yu, Z., Zhao, B., and
       Wei, J.: The Flexible Global Ocean-Atmosphere-Land System Model Grid-Point Version 3 (FGOALS-g3): Description and Evaluation,
       Journal of Advances in Modeling Earth Systems, 12, e2019MS002 012, https://doi.org/10.1029/2019MS002012, 2020.

López-Parages, J., Rodríguez-Fonseca, B., and Terray, L.: A mechanism for the multidecadal modulation of ENSO teleconnection with Europe, Climate Dynamics, 45, 867–880, https://doi.org/10.1007/s00382-014-2319-x, 2015.

665 Lorenz, D. J. and DeWeaver, E. T.: Tropopause height and zonal wind response to global warming in the IPCC scenario integrations, Journal of Geophysical Research: Atmospheres, 112, https://doi.org/https://doi.org/10.1029/2006JD008087, 2007.

Lorenz, D. J. and Hartmann, D. L.: Eddy–Zonal Flow Feedback in the Northern Hemisphere Winter, Journal of Climate, 16, 1212–1227, https://doi.org/https://doi.org/10.1175/1520-0442(2003)16<1212:EFFITN>2.0.CO;2, 2003.

Lü, J.-M., Kim, S.-J., Abe-Ouchi, A., Yu, Y., and Ohgaito, R.: Arctic Oscillation during the Mid-Holocene and Last Glacial Maximum from
670 PMIP2 Coupled Model Simulations, Journal of Climate, 23, 3792–3813, https://doi.org/https://doi.org/10.1175/2010JCLI3331.1, 2010.

Madan, G., Gjermundsen, A., Iversen, S. C., and LaCasce, J. H.: The weakening AMOC under extreme climate change, Climate Dynamics, 62, 1291–1309, https://doi.org/10.1007/s00382-023-06957-7, 2024.

Marino, G., Rohling, E. J., Rodríguez-Sanz, L., Grant, K. M., Heslop, D., Roberts, A. P., Stanford, J. D., and Yu, J.: Bipolar seesaw control on last interglacial sea level, Nature, 522, 197–201, https://doi.org/10.1038/nature14499, 2015.

675 Marshall, J., Johnson, H., and Goodman, J.: A Study of the Interaction of the North Atlantic Oscillation with Ocean Circulation, Journal of Climate, 14, 1399–1421, https://doi.org/https://doi.org/10.1175/1520-0442(2001)014<1399:ASOTIO>2.0.CO;2, 2001.

Mauri, A., Davis, B. A. S., Collins, P. M., and Kaplan, J. O.: The influence of atmospheric circulation on the mid-Holocene climate of Europe: a data–model comparison, Climate of the Past, 10, 1925–1938, https://doi.org/10.5194/cp-10-1925-2014, 2014.

Mauritsen, T., Bader, J., Becker, T., Behrens, J., Bittner, M., Brokopf, R., Brovkin, V., Claussen, M., Crueger, T., Esch, M., Fast, I., Fiedler,
680 S., Fläschner, D., Gayler, V., Giorgetta, M., Goll, D. S., Haak, H., Hagemann, S., Hedemann, C., Hohenegger, C., Ilyina, T., Jahns, T., Jimenéz-de-la Cuesta, D., Jungclaus, J., Kleinen, T., Kloster, S., Kracher, D., Kinne, S., Kleberg, D., Lasslop, G., Kornblueh, L., Marotzke, J., Matei, D., Meraner, K., Mikolajewicz, U., Modali, K., Möbis, B., Müller, W. A., Nabel, J. E. M. S., Nam, C. C. W., Notz, D., Nyawira, S.-S., Paulsen, H., Peters, K., Pincus, R., Pohlmann, H., Pongratz, J., Popp, M., Raddatz, T. J., Rast, S., Redler, R., Reick, C. H., Rohrschneider, T., Schemann, V., Schmidt, H., Schnur, R., Schulzweida, U., Six, K. D., Stein, L., Stemmler, I., Stevens, B., von
685 Storch, J.-S., Tian, F., Voigt, A., Vrese, P., Wieners, K.-H., Wilkenskjeld, S., Winkler, A., and Roeckner, E.: Developments in the MPI-M Earth System Model version 1.2 (MPI-ESM1.2) and Its Response to Increasing CO2, Journal of Advances in Modeling Earth Systems, 11, 998–1038, https://doi.org/https://doi.org/10.1029/2018MS001400, 2019.

Michel, S., Swingedouw, D., Chavent, M., Ortega, P., Mignot, J., and Khodri, M.: Reconstructing climatic modes of variability from proxy records using ClimIndRec version 1.0, Geoscientific Model Development, 13, 841–858, https://doi.org/10.5194/gmd-13-841-2020, 2020.

690 Miller, R. L., Schmidt, G. A., and Shindell, D. T.: Forced annular variations in the 20th century Intergovernmental Panel on Climate Change Fourth Assessment Report models, Journal of Geophysical Research: Atmospheres, 111, https://doi.org/https://doi.org/10.1029/2005JD006323, 2006.

Mosedale, T. J., Stephenson, D. B., Collins, M., and Mills, T. C.: Granger Causality of Coupled Climate Processes: Ocean Feedback on the North Atlantic Oscillation, Journal of Climate, 19, 1182 – 1194, https://doi.org/10.1175/JCLI3653.1, 2006.

695 Omrani, N.-E., Keenlyside, N., Matthes, K., Boljka, L., Zanchettin, D., Jungclaus, J. H., and Lubis, S. W.: Coupled stratosphere-troposphere-Atlantic multidecadal oscillation and its importance for near-future climate projection, npj Climate and Atmospheric Science, 5, 59, https://doi.org/10.1038/s41612-022-00275-1, 2022.

Osborn, T. J.: Simulating the winter North Atlantic Oscillation: the roles of internal variability and greenhouse gas forcing, Climate Dynamics, 22, 605–623, https://doi.org/10.1007/s00382-004-0405-1, 2004.

700 Otto-Bliesner, B. L., Brady, E. C., Clauzet, G., Tomas, R., Levis, S., and Kothavala, Z.: Last Glacial Maximum and Holocene Climate in
        CCSM3, Journal of Climate, 19, 2526–2544, https://doi.org/https://doi.org/10.1175/JCLI3748.1, 2006.

Otto-Bliesner, B. L., Braconnot, P., Harrison, S. P., Lunt, D. J., Abe-Ouchi, A., Albani, S., Bartlein, P. J., Capron, E., Carlson, A. E., Dutton,
        A., et al.: The PMIP4 contribution to CMIP6–Part 2: Two interglacials, scientific objective and experimental design for Holocene and Last
        Interglacial simulations, Geoscientific Model Development, 10, 3979–4003, https://doi.org/10.5194/gmd-10-3979-2017, 2017.

705 Otto-Bliesner, B. L., Brady, E. C., Tomas, R. A., Albani, S., Bartlein, P. J., Mahowald, N. M., Shafer, S. L., Kluzek, E., Lawrence, P. J., Leguy,
        G., Rothstein, M., and Sommers, A.: A Comparison of the CMIP6 midHolocene and lig127k Simulations in CESM2, Paleoceanography
        and Paleoclimatology, 35, e2020PA003 957, https://doi.org/https://doi.org/10.1029/2020PA003957, 2020.

Otto-Bliesner, B. L., Brady, E. C., Zhao, A., Brierley, C. M., Axford, Y., Capron, E., Govin, A., Hoffman, J. S., Isaacs, E., Kageyama, M.,
        Scussolini, P., Tzedakis, P. C., Williams, C. J. R., Wolff, E., Abe-Ouchi, A., Braconnot, P., Ramos Buarque, S., Cao, J., de Vernal, A., Guar-
710   ino, M. V., Guo, C., LeGrande, A. N., Lohmann, G., Meissner, K. J., Menviel, L., Morozova, P. A., Nisancioglu, K. H., O'ishi, R., Salas y
        Mélia, D., Shi, X., Sicard, M., Sime, L., Stepanek, C., Tomas, R., Volodin, E., Yeung, N. K. H., Zhang, Q., Zhang, Z., and Zheng, W.:
        Large-scale features of Last Interglacial climate: results from evaluating the *lig127k* simulations for the Coupled Model Intercomparison
        Project (CMIP6)–Paleoclimate Modeling Intercomparison Project (PMIP4), Climate of the Past, 17, 63–94, https://doi.org/10.5194/cp-
        17-63-2021, 2021.

715 Oudar, T., Sanchez-Gomez, E., Chauvin, F., Cattiaux, J., Terray, L., and Cassou, C.: Respective roles of direct GHG radiative forc-
        ing and induced Arctic sea ice loss on the Northern Hemisphere atmospheric circulation, Climate Dynamics, 49, 3693–3713,
        https://doi.org/10.1007/s00382-017-3541-0, 2017.

Park, W., Keenlyside, N., Latif, M., Ströh, A., Redler, R., Roeckner, E., and Madec, G.: Tropical Pacific Climate and Its Response to Global
        Warming in the Kiel Climate Model, Journal of Climate, 22, 71 – 92, https://doi.org/10.1175/2008JCLI2261.1, 2009.

720 Pedersen, R. A., Cvijanovic, I., Langen, P. L., and Vinther, B. M.: The Impact of Regional Arctic Sea Ice Loss on Atmospheric Circulation
        and the NAO, Journal of Climate, 29, 889–902, https://doi.org/https://doi.org/10.1175/JCLI-D-15-0315.1, 2016.

Peings, Y., Cattiaux, J., Vavrus, S., and Magnusdottir, G.: Late Twenty-First-Century Changes in the Midlatitude Atmospheric Circulation in
        the CESM Large Ensemble, Journal of Climate, 30, 5943–5960, https://doi.org/https://doi.org/10.1175/JCLI-D-16-0340.1, 2017.

Peltier, W. R., Argus, D. F., and Drummond, R.: Space geodesy constrains ice age terminal deglaciation: The global ICE-6G_C (VM5a)
725   model, Journal of Geophysical Research: Solid Earth, 120, 450–487, https://doi.org/https://doi.org/10.1002/2014JB011176, 2015.

Phipps, S., Rotstayn, L., Gordon, H., Roberts, J., Hirst, A., and Budd, W.: The CSIRO Mk3L climate system model version 1.0–Part 2:
        Response to external forcings, Geoscientific Model Development, 5, 649–682, https://doi.org/10.5194/gmd-5-649-2012, 2012.

Rimbu, N., Lohmann, G., Kim, J. H., Arz, H. W., and Schneider, R.: Arctic/North Atlantic Oscillation signature in Holocene sea surface tem-
        perature trends as obtained from alkenone data, Geophysical Research Letters, 30, https://doi.org/https://doi.org/10.1029/2002GL016570,
730   2003.

Rind, D., Perlwitz, J., and Lonergan, P.: AO/NAO response to climate change: 1. Respective influences of stratospheric and tropospheric
        climate changes, Journal of Geophysical Research: Atmospheres, 110, https://doi.org/https://doi.org/10.1029/2004JD005103, 2005a.

Rind, D., Perlwitz, J., Lonergan, P., and Lerner, J.: AO/NAO response to climate change: 2. Relative importance of low- and high-latitude
        temperature changes, Journal of Geophysical Research: Atmospheres, 110, https://doi.org/https://doi.org/10.1029/2004JD005686, 2005b.

735 Rotstayn, L. D., Collier, M. A., Mitchell, R. M., Qin, Y., Campbell, S. K., and Dravitzki, S. M.: Simulated enhancement of ENSO-related
        rainfall variability due to Australian dust, Atmospheric Chemistry and Physics, 11, 6575–6592, https://doi.org/10.5194/acp-11-6575-2011,
        2011.

Schmidt, G. A., Kelley, M., Nazarenko, L., Ruedy, R., Russell, G. L., Aleinov, I., Bauer, M., Bauer, S. E., Bhat, M. K., Bleck, R., Canuto,
V., Chen, Y.-H., Cheng, Y., Clune, T. L., Del Genio, A., de Fainchtein, R., Faluvegi, G., Hansen, J. E., Healy, R. J., Kiang, N. Y., Koch,
740   D., Lacis, A. A., LeGrande, A. N., Lerner, J., Lo, K. K., Matthews, E. E., Menon, S., Miller, R. L., Oinas, V., Oloso, A. O., Perlwitz, J. P.,
Puma, M. J., Putman, W. M., Rind, D., Romanou, A., Sato, M., Shindell, D. T., Sun, S., Syed, R. A., Tausnev, N., Tsigaridis, K., Unger,
N., Voulgarakis, A., Yao, M.-S., and Zhang, J.: Configuration and assessment of the GISS ModelE2 contributions to the CMIP5 archive,
Journal of Advances in Modeling Earth Systems, 6, 141–184, https://doi.org/10.1002/2013MS000265, 2014.

Screen, J. A., Bracegirdle, T. J., and Simmonds, I.: Polar Climate Change as Manifest in Atmospheric Circulation, Current Climate Change
745   Reports, 4, 383–395, https://doi.org/10.1007/s40641-018-0111-4, 2018.

Seland, Ø., Bentsen, M., Seland Graff, L., Olivié, D., Toniazzo, T., Gjermundsen, A., Debernard, J. B., Gupta, A. K., He, Y., Kirkevåg,
A., Schwinger, J., Tjiputra, J., Schancke Aas, K., Bethke, I., Fan, Y., Griesfeller, J., Grini, A., Guo, C., Ilicak, M., Hafsahl Karset, I. H.,
Landgren, O., Liakka, J., Onsum Moseid, K., Nummelin, A., Spensberger, C., Tang, H., Zhang, Z., Heinze, C., Iverson, T., and Schulz,
M.: The Norwegian Earth System Model, NorESM2 – Evaluation of theCMIP6 DECK and historical simulations, Geoscientific Model
750   Development Discussions, 2020, 1–68, https://doi.org/10.5194/gmd-2019-378, 2020.

Serreze, M. C. and Barry, R. G.: Processes and impacts of Arctic amplification: A research synthesis, Global and Planetary Change, 77,
85–96, https://doi.org/https://doi.org/10.1016/j.gloplacha.2011.03.004, 2011.

Shi, X., Werner, M., Yang, H., D'Agostino, R., Liu, J., Yang, C., and Lohmann, G.: Unraveling the complexities of the Last Glacial Maximum
climate: the role of individual boundary conditions and forcings, Climate of the Past, 19, 2157–2175, https://doi.org/10.5194/cp-19-2157-
755   2023, 2023.

Sidorenko, D., Rackow, T., Jung, T., Semmler, T., Barbi, D., Danilov, S., Dethloff, K., Dorn, W., Fieg, K., Goessling, H. F., Handorf, D.,
Harig, S., Hiller, W., Juricke, S., Losch, M., Schröter, J., Sein, D. V., and Wang, Q.: Towards multi-resolution global climate modeling
with ECHAM6?FESOM. Part I: model formulation and mean climate, Climate Dynamics, 44, 757–780, https://doi.org/10.1007/s00382-
014-2290-6, 2015.

760   Slivinski, L. C., Compo, G. P., Whitaker, J. S., Sardeshmukh, P. D., Giese, B. S., McColl, C., Allan, R., Yin, X., Vose, R., Titchner, H.,
Kennedy, J., Spencer, L. J., Ashcroft, L., Brönnimann, S., Brunet, M., Camuffo, D., Cornes, R., Cram, T. A., Crouthamel, R., Domínguez-
Castro, F., Freeman, J. E., Gergis, J., Hawkins, E., Jones, P. D., Jourdain, S., Kaplan, A., Kubota, H., Blancq, F. L., Lee, T.-C., Lorrey, A.,
Luterbacher, J., Maugeri, M., Mock, C. J., Moore, G. K., Przybylak, R., Pudmenzky, C., Reason, C., Slonosky, V. C., Smith, C. A., Tinz,
B., Trewin, B., Valente, M. A., Wang, X. L., Wilkinson, C., Wood, K., and Wyszyński, P.: Towards a more reliable historical reanalysis:
765   Improvements for version 3 of the Twentieth Century Reanalysis system, Quarterly Journal of the Royal Meteorological Society, 145,
2876–2908, https://doi.org/https://doi.org/10.1002/qj.3598, 2019.

Smith, D. M., Dunstone, N. J., Scaife, A. A., Fiedler, E. K., Copsey, D., and Hardiman, S. C.: Atmospheric Response to Arctic and
Antarctic Sea Ice: The Importance of Ocean–Atmosphere Coupling and the Background State, Journal of Climate, 30, 4547–4565,
https://doi.org/https://doi.org/10.1175/JCLI-D-16-0564.1, 2017.

770   Spencer, M. and Essery, R.: Scottish snow cover dependence on the North Atlantic Oscillation index, Hydrology Research, 47, 619–629,
https://doi.org/10.2166/nh.2016.085, 2016.

Stephenson, D. B., Pavan, V., Collins, M., Junge, M. M., Quadrelli, R., and Groups, P. C. M.: North Atlantic Oscillation response to transient
greenhouse gas forcing and the impact on European winter climate: a CMIP2 multi-model assessment, Climate Dynamics, 27, 401–420,
https://doi.org/10.1007/s00382-006-0140-x, 2006.

775 Sueyoshi, T., Ohgaito, R., Yamamoto, A., Chikamoto, M. O., Hajima, T., Okajima, H., Yoshimori, M., Abe, M., O'ishi, R., Saito, F., Watan-
abe, S., Kawamiya, M., and Abe-Ouchi, A.: Set-up of the PMIP3 paleoclimate experiments conducted using an Earth system model,
MIROC-ESM, Geoscientific Model Development, 6, 819–836, https://doi.org/10.5194/gmd-6-819-2013, 2013.

Taylor, K. E., Stouffer, R. J., and Meehl, G. A.: An Overview of CMIP5 and the Experiment Design, Bulletin of the American Meteorological
Society, 93, 485–498, https://doi.org/10.1175/BAMS-D-11-00094.1, 2012.

780 Thompson, D. and Wallace, J.: The Arctic oscillation signature in the wintertime geopotential height and temperature fields, Geophysical
Research Letters, 25, 1297–1300, https://doi.org/10.1029/98gl00950, 1998.

Toniazzo, T. and Scaife, A. A.: The influence of ENSO on winter North Atlantic climate, Geophysical Research Letters, 33,
https://doi.org/https://doi.org/10.1029/2006GL027881, 2006.

Vallis, G. K., Zurita-Gotor, P., Cairns, C., and Kidston, J.: Response of the large-scale structure of the atmosphere to global warming,
785 Quarterly Journal of the Royal Meteorological Society, 141, 1479–1501, https://doi.org/https://doi.org/10.1002/qj.2456, 2015.

Vinther, B. M., Andersen, K. K., Hansen, A. W., Schmith, T., and Jones, P. D.: Improving the Gibraltar/Reykjavik NAO index, Geophysical
Research Letters, 30, https://doi.org/10.1029/2003GL018220, 2003.

Voldoire, A., Sanchez-Gomez, E., y Mélia, D. S., Decharme, B., Cassou, C., Sénési, S., Valcke, S., Beau, I., Alias, A., Chevallier, M., Déqué,
M., Deshayes, J., Douville, H., Fernandez, E., Madec, G., Maisonnave, E., Moine, M.-P., Planton, S., Saint-Martin, D., Szopa, S., Tyteca,
790 S., Alkama, R., Belamari, S., Braun, A., Coquart, L., and Chauvin, F.: The CNRM-CM5. 1 global climate model: description and basic
evaluation, Climate Dynamics, 40, 2091–2121, https://doi.org/10.1007/s00382-011-1259-y, 2013.

Volodin, E. M., Mortikov, E. V., Kostrykin, S. V., Galin, V. Y., Lykossov, V. N., Gritsun, A. S., Diansky, N. A., Gusev, A. V., Iakovlev,
N. G., Shestakova, A. A., and Emelina, S. V.: Simulation of the modern climate using the INM-CM48 climate model, Russian Journal of
Numerical Analysis and Mathematical Modelling, 33, 367–374, https://doi.org/10.1515/rnam-2018-0032, 2018.

795 Walker, G. and Bliss, E.: World Weather V, Memoirs of the Royal Meteorological Society, 4, 53–84, 1932.

Wang, L. and Ting, M.: Stratosphere-Troposphere Coupling Leading to Extended Seasonal Predictability of Summer North Atlantic Oscil-
lation and Boreal Climate, Geophysical Research Letters, 49, e2021GL096 362, https://doi.org/https://doi.org/10.1029/2021GL096362,
2022.

Waskom, M. L.: seaborn: statistical data visualization, Journal of Open Source Software, 6, 3021, https://doi.org/10.21105/joss.03021, 2021.

800 Williams, K. D., Copsey, D., Blockley, E. W., Bodas-Salcedo, A., Calvert, D., Comer, R., Davis, P., Graham, T., Hewitt, H. T., Hill, R., Hyder,
P., Ineson, S., Johns, T. C., Keen, A. B., Lee, R. W., Megann, A., Milton, S. F., Rae, J. G. L., Roberts, M. J., Scaife, A. A., Schiemann,
R., Storkey, D., Thorpe, L., Watterson, I. G., Walters, D. N., West, A., Wood, R. A., Woollings, T., and Xavier, P. K.: The Met Office
Global Coupled Model 3.0 and 3.1 (GC3.0 and GC3.1) Configurations, Journal of Advances in Modeling Earth Systems, 10, 357–380,
https://doi.org/https://doi.org/10.1002/2017MS001115, 2018.

805 Woollings, T., Czuchnicki, C., and Franzke, C.: Twentieth century North Atlantic jet variability, Quarterly Journal of the Royal Meteorolog-
ical Society, 140, 783–791, https://doi.org/https://doi.org/10.1002/qj.2197, 2014.

Woollings, T., Franzke, C., Hodson, D. L. R., Dong, B., Barnes, E. A., Raible, C. C., and Pinto, J. G.: Contrasting interannual and multidecadal
NAO variability, Climate Dynamics, 45, 539–556, https://doi.org/10.1007/s00382-014-2237-y, 2015.

Xin, X., Wu, T., Li, J., Wang, Z., Li, W., and Wu, F.: How Well does BCC_CSM1.1 Reproduce the 20th Century Climate Change over
810 China?, Atmospheric and Oceanic Science Letters, 6, 21–26, https://doi.org/10.1080/16742834.2013.11447053, 2013.

Yoshimori, M. and Suzuki, M.: The relevance of mid-Holocene Arctic warming to the future, Climate of the Past, 15, 1375–1394,
https://doi.org/10.5194/cp-15-1375-2019, 2019.

Yukimoto, S., Adachi, Y., Hosaka, M., Sakami, T., Yoshimura, H., Hirabara, M., Tanaka, T. Y., Shindo, E., Tsujino, H., Deushi, M., Mizuta, R., Yabu, S., Obata, A., Nakano, H., Koshiro, T., Ose, T., and Kitoh, A.: A new global climate model of the Meteorological Research

815   Institute: MRI-CGCM3—model description and basic performance, Journal of the Meteorological Society of Japan. Ser. II, 90, 23–64, https://doi.org/10.2151/jmsj.2012-A02, 2012.

Yukimoto, S., Kawai, H., Koshiro, T., Oshima, N., Yoshida, K., Urakawa, S., Tsujino, H., Deushi, M., Tanaka, T., Hosaka, M., Yabu, S., Yoshimura, H., Shindo, E., Mizuta, R., Obata, A., Adachi, Y., and Ishii, M.: The Meteorological Research Institute Earth System Model Version 2.0, MRI-ESM2. 0: Description and Basic Evaluation of the Physical Component, Journal of the Meteorological Society of Japan.

820   Ser. II, 97, 931–965, https://doi.org/10.2151/jmsj.2019-051, 2019.

Zelinka, M. D., Myers, T. A., McCoy, D. T., Po-Chedley, S., Caldwell, P. M., Ceppi, P., Klein, S. A., and Taylor, K. E.: Causes of Higher Climate Sensitivity in CMIP6 Models, Geophysical Research Letters, 47, e2019GL085 782, https://doi.org/https://doi.org/10.1029/2019GL085782, 2020.

Zhang, Q., Liu, B., Li, S., and Zhou, T.: Understanding Models' Global Sea Surface Temperature Bias in Mean State: From CMIP5 to

825   CMIP6, Geophysical Research Letters, 50, e2022GL100 888, https://doi.org/https://doi.org/10.1029/2022GL100888, 2023.

Zhang, W., Wang, L., Xiang, B., Qi, L., and He, J.: Impacts of two types of La Niña on the NAO during boreal winter, Climate Dynamics, 44, 1351–1366, https://doi.org/10.1007/s00382-014-2155-z, 2015.

Zhang, W., Wang, Z., Stuecker, M. F., Turner, A. G., Jin, F.-F., and Geng, X.: Impact of ENSO longitudinal position on teleconnections to the NAO, Climate Dynamics, 52, 257–274, https://doi.org/10.1007/s00382-018-4135-1, 2019.

830 Zhao, A., Brierley, C. M., Jiang, Z., Eyles, R., Oyarzún, D., and Gomez-Dans, J.: Analysing the PMIP4-CMIP6 collection: a workflow and tool (pmip_p2fvar_analyzer v1), Geoscientific Model Development, 15, 2475–2488, https://doi.org/10.5194/gmd-15-2475-2022, 2022.

Zhu, C., Liu, Z., Zhang, S., and Wu, L.: Likely accelerated weakening of Atlantic overturning circulation emerges in optimal salinity fingerprint, Nature Communications, 14, 1245, https://doi.org/10.1038/s41467-023-36288-4, 2023.

Figure 1. Comparison between observations (left column) taken from the 20th-Century Reanalysis (Slivinski et al., 2019) and the ensemble mean of the *piControl* (right column). Panels show DJF mean variables over the North Atlantic sector (see Sect. 2.3 for region definition). The rows present the sea surface temperatures (a, b), precipitation (c, d), sea level pressure (e, f), NAO pattern (g, h), and teleconnections between NAO and temperature (i, j) and precipitation (k, l) computed by regression against the NAO.
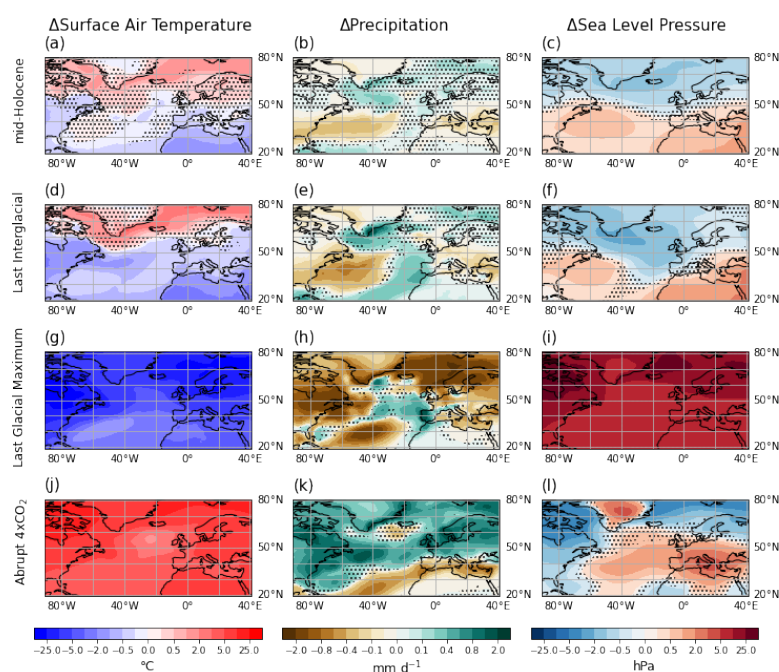
Figure 2. Ensemble mean change in mean states. The columns from left to right show the DJF mean surface air temperature (°C; a, d ,g, j), precipitation (mm d^{-1}; b, e, h, k) and sea level pressure (hPa; c, f, i l). The rows show the ensemble mean difference from the *piControl* simulations for the *midHolocene* (a, b, c), *lig127k* (d, e, f), *lgm* (g, h, i), and *abrupt4xCO2* simulations (j, k, l). Stippling indicates where the ensemble is inconsistent in the direction of change.
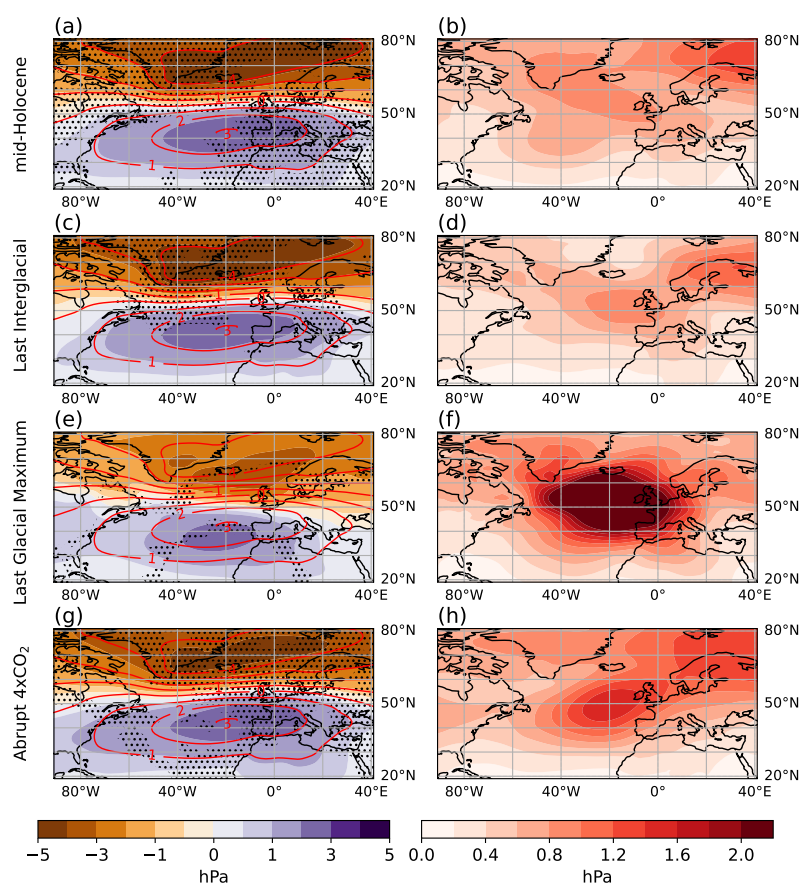
Figure 3. SLP spatial pattern for NAO in DJF (hPa) in each experiment, including the *midHolocene* (a), *lig127k* (c), *lgm* (e) and *abrupt4xCO2*(g). Red contours represent the pattern of the *piControl*, and stippling indicates where the ensemble is inconsistent in the direction of change. Ensemble variation is presented as the standard deviation across the ensemble (b, d, f, h).
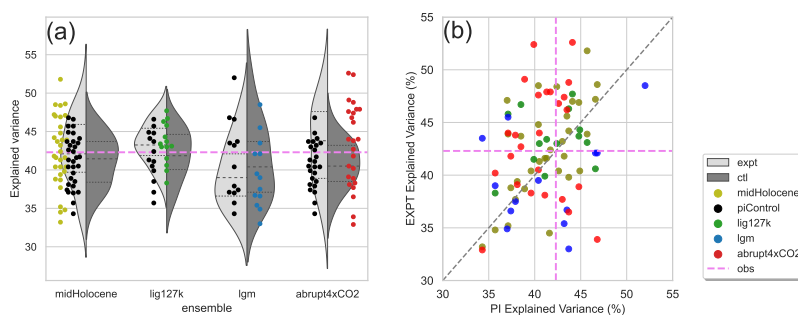
Figure 4. Total variance explained by the NAO for (a) the experiments and (b) comparison with the *piControl*. (a) For each column, the dots (corresponding to the left y-axis) show the explained variance by models. The distributions are computed via a kernel density estimation (Waskom, 2021): The curves show the distributions of the explained variance by models for each experiment (left) and the *piControl* (right); horizontal dashed and dotted lines represent the median and 75% and 25% quartiles, respectively. The horizontal location of dots within each column does not have any meaning.
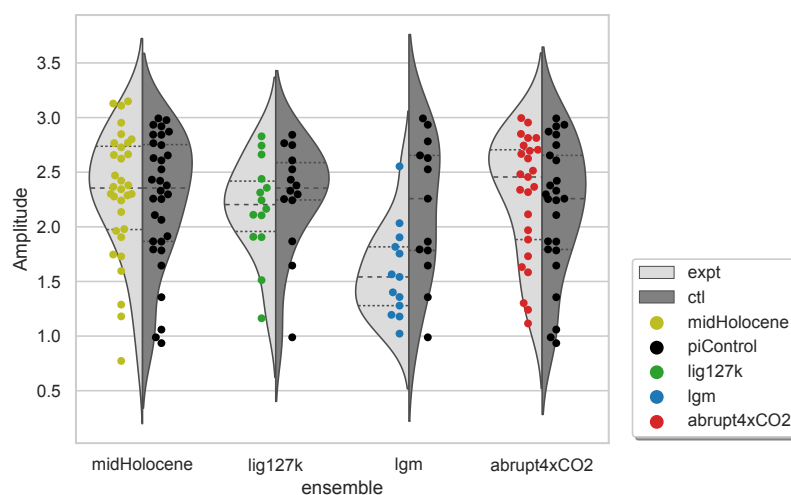
Figure 5. The NAO amplitude (hPa) for the experiments. The amplitude is measured as the standard deviation of the renormalised NAO PC time series (Sect. 2.3.).
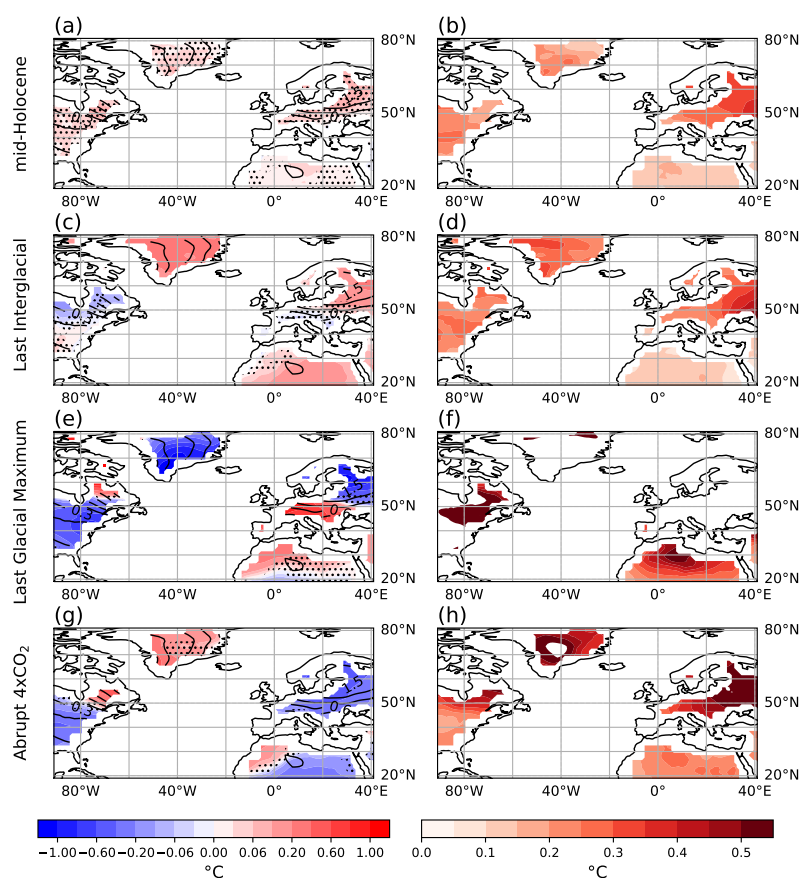
Figure 6. Same as Figure 3 but for ensemble mean change in DJF surface mean temperature (°C) associated with the NAO. Stippling indicates where the ensemble is inconsistent in the direction of change.
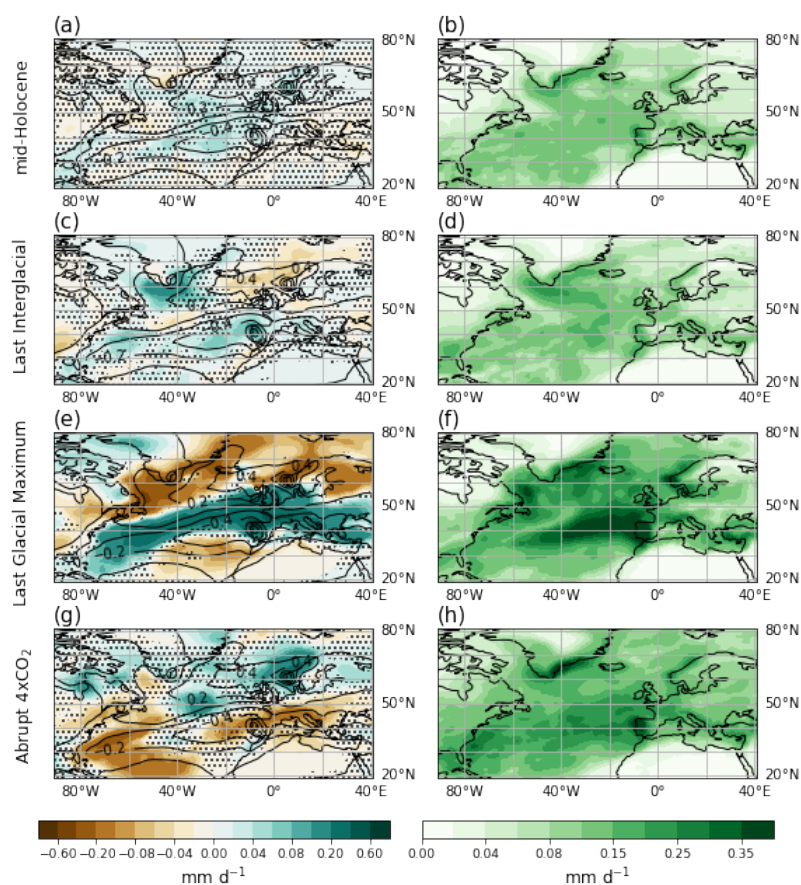
Figure 7. Same as Figure 3 but for ensemble mean change in DJF precipitation (mm d^{-1} associated with the NAO. Stippling indicates where the ensemble is inconsistent in the direction of change.
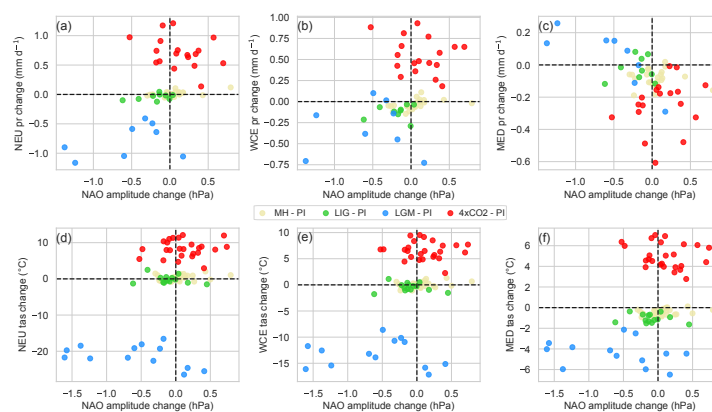
Figure 8. Relationships across all experiments and all models between the changes in NAO amplitude and the changes in European mean state of DJF mean precipitation (mm d^{-1}; labelled as pr in panels a to c) and surface temperature (°C; labelled as tas in panels d to f). Regions follow the definition of IPCC AR6: northern Europe is referred to as NEU, west and central Europe as WCE and Mediterranean MED. All changes are relative to the *piControl*.
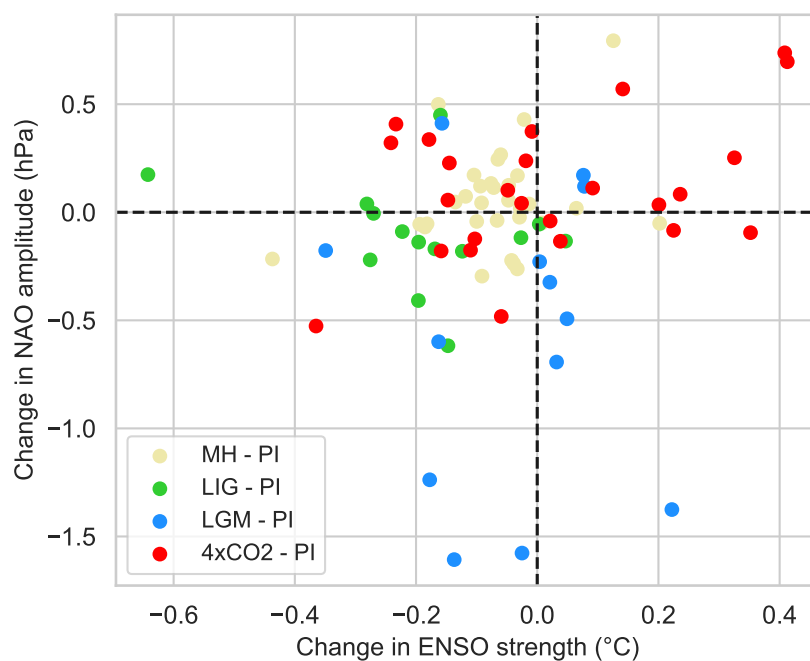
Figure 9. Relationship between the change in ENSO strength and NAO amplitude across all models and all experiments relative to the *piControl*. The ENSO strength is measured as the standard deviation of the nino3.4 index of each simulation.

Table 1. Models contributing to the control experiment (*piControl*), the PMIP experiments (*midHolocene* (MH); *lig127k* (LIG); *lgm* (LGM)) and an idealised CO_2 experiments (*abrupt4xCO2* (4xCO2)) under the CMIP5 and the CMIP6. Numbers in Participation represent the length of model years of each simulation.

Model	PMIP	ECS* (K)	Participation					REF.
			PI	MH	LIG	LGM	abrupt4xCO2	
AWI-ESM-1-1-LR	4	3.6	100	100	100	100		Sidorenko et al. (2015)
BCC-CSM1-1	3	3.1	500	100			50	Xin et al. (2013)
CCSM4	3	2.9	1051	301		101	50	Gent et al. (2011)
CESM2	4	5.3	500	700			50	Gettelman et al. (2019)
CNRM-CM5	3	3.3	850	200		200	50	Voldoire et al. (2013)
CNRM-CM6-1	4	5.1	500		301		50	Craig et al. (2017)
COSMOS-ASO	3		399			600		Wetzel et al. (2010)
CSIRO-Mk3-6-0	3	4.1	500	100			50	Rotstayn et al. (2011)
CSIRO-Mk3L-1-2	3	3.1	1000	500				Phipps et al. (2012)
EC-EARTH-2-2	3	4.2	40	40				Hazeleger et al. (2012)
EC-Earth3-LR	4	4.3	201	203	210			Döscher et al. (2021)
FGOALS-f3-L	4	3	561	500	500		50	He et al. (2020)
FGOALS-g2	3	3.7	700	680		100	50	Li et al. (2013)
FGOALS-g3	4	2.9	700	500	500			Li et al. (2020)
FGOALS-s2	3	4.5	501	100			50	Bao et al. (2013)
GISS-E2-1-G	4	2.7	851	100	100		50	Kelley et al. (2020)
GISS-E2-R	3	2.1	500	100		100	50	Schmidt et al. (2014)
HadGEM2-CC	3	4.5	240	35				Collins et al. (2011)
HadGEM2-ES	3	4.6	336	101			50	Collins et al. (2011)
HadGEM3-GC31-LL	4	5.4	100	100	200			Williams et al. (2018)
INM-CM4-8	4	2.1	531	200	100	200	50	Volodin et al. (2018)
IPSL-CM5A-LR	3	4.1	1000	500		200	50	Dufresne et al. (2013)
IPSL-CM6A-LR	4	4.5	1200	550	550		50	Boucher et al. (2020)
KCM1-2-2	3		200	100				Park et al. (2009)
MIROC-ES2L	4	2.7	500	100	100	100	50	Hajima et al. (2020)
MIROC-ESM	3	4.7	630	100		100	50	Sueyoshi et al. (2013)
MPI-ESM-P	3	3.5	1156	100		100	50	Giorgetta et al. (2013)
MPI-ESM1-2-LR	4	2.8	1000	500	300		50	Mauritsen et al. (2019)
MRI-CGCM3	3	2.6	500	100		100	50	Yukimoto et al. (2012)
MRI-ESM2-0	4	3.1	701	200			50	Yukimoto et al. (2019)
NESM3	4	3.7	100	100	100		50	Cao et al. (2018)
NorESM1-F	4	2.3	200	200	200			Guo et al. (2019)
NorESM2-LM	4	2.5	391	100	100		50	Seland et al. (2020)
UofT-CCSM-4	4	3.2	100	100		100		Chandan and Peltier (2017)
Ensemble size			34	32	14	13	23	